SYNTHESIS AND CHARACTERIZATION OF MAGHEMITE NANOPARTICLES DEPOSITED ON SILICON SUBSTRATE

NURUL ATHIRAH BINTI ABU HUSSEIN

FACULTY OF ENGINEERING
UNIVERSITY OF MALAYA
KUALA LUMPUR

2018

SYNTHESIS AND CHARACTERIZATION OF MAGHEMITE NANOPARTICLES DEPOSITED ON SILICON SUBSTRATE

NURUL ATHIRAH BINTI ABU HUSSEIN

DISSERTATION SUBMITTED IN FULFILMENT OF THE REQUIREMENTS FOR THE DEGREE OF MASTER OF ENGINEERING SCIENCE

**FACULTY OF ENGINEERING
UNIVERSITY OF MALAYA
KUALA LUMPUR**

2018

UNIVERSITY OF MALAYA
ORIGINAL LITERARY WORK DECLARATION

Name of Candidate: Nurul Athirah binti Abu Hussein

(I.C/Passport No:

Matric No: KGA 140047

Name of Degree: Master of Engineering Science

Title of Project Paper/Research Report/Dissertation/Thesis ("this Work"):

Synthesis and Characterization of Maghemite Nanoparticle Deposited on Silicon Substrate

Field of Study: Advance Materials/Nanomaterials (Materials Engineering)

I do solemnly and sincerely declare that:

(1) I am the sole author/writer of this Work;
(2) This Work is original;
(3) Any use of any work in which copyright exists was done by way of fair dealing and for permitted purposes and any excerpt or extract from, or reference to or reproduction of any copyright work has been disclosed expressly and sufficiently and the title of the Work and its authorship have been acknowledged in this Work;
(4) I do not have any actual knowledge nor do I ought reasonably to know that the making of this work constitutes an infringement of any copyright work;
(5) I hereby assign all and every rights in the copyright to this Work to the University of Malaya ("UM"), who henceforth shall be owner of the copyright in this Work and that any reproduction or use in any form or by any means whatsoever is prohibited without the written consent of UM having been first had and obtained;
(6) I am fully aware that if in the course of making this Work I have infringed any copyright whether intentionally or otherwise, I may be subject to legal action or any other action as may be determined by UM.

Candidate's Signature Date:

Subscribed and solemnly declared before,

Witness's Signature Date:

Name:

Designation:

SYNTHESIS AND CHARACTERIZATION OF MAGHEMITE NANOPARTICLES DEPOSITED ON SILICON SUBSTRATE

ABSTRACT

This study comprised of two stages. In the first stage, pure maghemite nanoparticles within the size range of 10 nm were synthesized where at the second stage, the as-synthesized maghemite nanoparticles were deposited on silicon substrate and annealed at different temperature. In the first stage, the effect of varying ferric nitrate concentration (0.1, 0.3, 0.5, 0.7 and 1.0 M) on the size and magnetic properties of iron oxide nanoparticles were investigated. From X-ray diffraction analysis (XRD), the peaks and the lattice parameter obtained indicated that the nanoparticles formed were maghemite (γ-Fe_2O_3). It was then further confirmed by Raman analysis. The magnetization curve pointed out that the particles were super paramagnetic nanoparticles as there were no hysteresis loops found. The crystallite, magnetic and physical size of the nanoparticles were similar indicated that they were monocrystals. As the concentration of ferric nitrate increased from 0.1 M to 0.5 M, the size of the as-synthesized maghemite nanoparticles decreased. However, as the concentration of ferric nitrate was further increased, the size of the nanoparticles was increasing as well. This occurrence was due to the agglomeration of the high surface energy of the nanosized particles. The smallest size of the maghemite nanoparticles with the physical size of 6.90 nm was chosen for the next stage. In the second stage, 1 cm x 1 cm n-type silicon substrate was cleaned using RCA method. After that, 40 µl of the selected maghemite nanoparticles were deposited onto the silicon substrate using micropipette and were spin coated at 2500 rpm for 1 minute. The samples were then annealed at different temperatures which were 600°C, 700°C, 800°C and 900°C. The effects of different annealing temperatures were investigated. Physical characterizations were conducted through the analysis of x-ray diffractometer (XRD), raman analysis, atomic force microscopy (AFM) and electrical properties. XRD analysis revealed that the thin layer of maghemite nanoparticles on the silicon substrate was stable and was confirmed by Raman analysis. The thickness of the maghemite nanoparticles layer was investigated through AFM analysis. It was revealed that the thickness was approximately 25 nm. The maghemite nanoparticles were seen to be distributed homogeneously on the silicon substrate. The electrical properties of the samples were investigated through current density-electrical field (J-E) analysis. This study revealed that different annealing temperature yield a different electrical behaviour. This is mainly due to the grain size of the nanoparticles after annealing process, surface roughness behaviour, distribution and porosity of the nanoparticles, and also the thickness of the thin film maghemite nanoparticles.

Keywords: Maghemite Nanoparticles, Massart's Procedure, Thin Film, Spin Coating, Electrical Analysis.

SINTESIS DAN PERINCIAN NANOPARTIKEL MAGHEMITE YANG DIDEPOSITKAN PADA SUBSTRAT SILIKON

ABSTRAK

Kajian ini terdiri daripada dua tahap. Tahap pertama terdiri daripada penghasilan maghemite nanopartikel yang tulen dengan saiz dalam lingkungan 10 nm manakala tahap kedua ialah dimana pemendapan maghemite nanopartikel ke atas substrat silikon dan kemudiannya dipanaskan pada suhu yang berbeza. Pada tahap pertama, kesan daripada perbezaan kepekatan nitrat ferik terhadap saiz dan sifat magnet iron oxide nanopartikel adalah disiasat. Berdasarkan analisis X-ray diffraction (XRD), puncak graf dan parameter kekisi yang diperoleh menunjukkan bahawa nanopartikel yang terhasil adalah maghemite nanopartikel (γ-Fe_2O_3). Ia kemudiannya disahkan oleh Raman analisis. Lengkungan magnet manunjukkan bahawa partikel tersebut adalah superparamagnetik nanopartikel kerana tiada gelung histeresis yang terhasil. Saiz crystallite, saiz magnetic dan saiz fizikal nanopartikel tersebut adalah lebih kurang sama membuktikan bahawa nanopartikel tersebut adalah monokristal. Peningkatan kepekatan nitrat ferik daripada 0.1M kepada 0.5M menghasilkan saiz nanopartikel yang semakin mengecil. Walaubagaimanapun, jika kepekatan nitrat ferik terus meningkat, saiz maghemite nanopartikel yang terhasil akan bertambah besar. Hal ini adalah berkemungkinan disebabkan oleh pergumpalan daripada nano partikel-nanopartikel yang dihasilkan. Maghemite nanopartikel dengan saiz yang paling kecil telah dipilih untuk digunakan pada tahap seterusnya. Pada tahap kedua, 1 cm x 1 cm substrat silikon jenis n telah dibersihkan menggunakan kaedah RCA. Kemudian, 40 µl maghemite nanopartikel yang terpilih telah dimendapkan ke atas substrat silikon menggunakan mikropipet dan di spin coat pada rpm 2500 selama 1 min. Sample tersebut kemudiannya dikuatkan dengan memanaskannya pada suhu yang berbeza-beza dan kesan terhadap perbezaan suhu ke atas substrat silikon telah disiasat.. Perincian fizikal telah dijalankan iaitu analisis x-ray diffratometer (XRD), raman analisis dan atomic force microscopy (AFM). Analisis XRD menunjukkan bahawa lapisan nipis maghemite nanopartikel di atas permukaan substrat silicon adalah stabil dan ianya disahkan oleh analisis raman. Ketebalan lapisan maghemite nanopartikel tersebut disiasat melalui analisis AFM. Ujian-ujian tersebut mendedahkan bahawa ketebalan lapisan maghemite tersebut ialah lebih kurang 25 nm. Taburan nanopartikel di atas substrat silikon menunjukkan bahawa ianya sekata. Struktur metal-oxide-semiconductor (MOS) ini telah direka cipta untuk menguji sifat elektrikal maghemite nanopartikel di atas substrat silikon. Sifat elektikal sample sample tersebut telah diuji melalui analisis current density-electric field (J-E). Kajian ini membuktikan bahawa perilaku elektrik adalah berbeza pada semua sampel yang dpanaskan pada suhu yang berbeza. Hal ini adalah disebakan oleh factor size butiran maghemite nanopartikel setelah proses pemanasan dijalankan, kekasaran permukaan sampel sample tersebut, distribusi maghemite nanopartikel dan liang liang pada pada silikon substrat dan juga ketebalan filem nipis maghemite nanopartikel tersebut.

Kata kunci: Nanopartikel Maghemite, Prosedur Massart, Filem Nipis, Salutan Spin, Analisis Elektrik.

ACKNOWLEDGEMENTS

I would like to express my gratitude to all those who have given me the possibility to complete my Master Degree of Science Engineering. First and foremost, heartfelt appreciation goes to my thesis advisors Assc. Prof. Ir. Dr. Ang Bee Chin, Ir. Dr. Wong Yew Hoong and Associate Professor Dr. Ong Boon Hoong. The door to their office was always open whenever I ran into trouble spot or had questions about my research or writing. They always guided and steered me in the right direction whenever I needed it.

I would also like to thank the experts who were involved in the research project: Mr. Said bin Sakat, senior laboratory assistant of Ceramic Processing Laboratory, Faculty of Engineering, Puan Zurina Marzuki and Mr. Amir Shah, person in-charge of Material Characterization Laboratory, Faculty of Science, Mr. Zaharudin bin Mohd. Salleh, laboratory assistant of X-ray Laboratory, Department of Geology, Faculty of Science, Madam Siew Siew, Mr. Lam and Mr. Tok from Hi-Tech Instruments Sdn. Bhd. Without their passionate participation and input, the research could not have been successfully conducted.

I am grateful for the financial support provided by University of Malaya’s PPP Grant No. PG151-2015A.

Finally, I must express my very profound gratitude to my parents and my colleagues for providing me with unfailing support and continuous encouragement throughout my years of study and through process of researching and writing this thesis. This accomplishment would not have been possible without them. Thank you.

TABLE OF CONTENTS

LIST OF FIGURES

LIST OF TABLES

LIST OF SYMBOLS AND ABBREVIATIONS

nm	Nanometre
g	Gram
cm	Centimetre
mg	Milligram
cm^{-1}	Per centimeter
g/cm^{2}	Gram per cenimetre square
m^{2}/g	Metre square per gram
A/cm^{2}	Ampere per centimeter square
%	Percentage
s^{-1}	Per second
°	Degree
2θ	Two theta
π	Pi
Å	Angstrom
kOe	Kilo oersted
mW	Miliwatt
V	Volt
a	Lattice parameter
Ms	Magnetic saturation
M	Molar
k	Boltzmann constant
T	Room temperature
K	Kelvin
pH	Potential of hydrogen

μl : Micro littre

°C : Degree celcius

κ : Kappa

eV : Electron volt

rpm : Rotation per minute

B : Flux density

H : Magnetic force

RCA : Radio corporation of america

R&D : Research and development

MOS : Metal oxide semiconductor

XRD : X-ray diffraction

TGA : Thermogravimetric analysis

BET : Brunauer-emmett-teller

AGM : Alternating gradient magnetometer

TEM : Transmission electron microscopy

γ-Fe_2O_3 : Maghemite

α-$FeO(OH)$: Geothite

γ-$FeO(OH)$: Lepidocrite

β-$FeO(OH,Cl)$: Akaganite

$Fe_8O_8(OH)_6(SO)_4.nH_2O$: Schwertmannite

$FeO(OH)$: Ferroxyhyte

$Fe_{10}O_{14}(OH)_2$: Ferrihydrite

$Fe(OH)_3.nH_2O$: Bernalite

Fe_2O_4 : Magnetite

α-Fe_2O_3 : Hematite

FeO : Wustite

$FeCl_2$: Ferrous chloride

$FeCl_3$: Ferric chloride

$Fe(NO_3)_3.9H_2O$: Ferric nitrate

Si : Silicon

Ge : Germanium

GeO_2 : Germanium dioxide

HfO_2 : Hafnium oxide

SiN_4 : Silicon nitride

ZrO_2 : Zirconium oxide

Al_2O_3 : Aluminium oxide

Ta_2O_5 : Tantalum oxide

$FeCl_3.6H_2O$: Ferric chloride hexahydrate

$FeCl_3.4H_2O$: Ferrous chloride tetrahydrate

HCl : Hydrocloric acid

HNO_3 : Nitric acid

NH_4OH : Ammonium hydroxide

H_2O_2 : Hydrogen peroxide

HF : Hydrofluoric acid

JFET : Junction gate field effect transistor

SIT : Static induction transistor

PVD : Physical vapor deposition

CVD : Chemical vapor deposition

KBr : Potassium bromide

CHAPTER 1: INTRODUCTION

1.1 Background and Problem Statement

Nanotechnology can be described as controlling matter at nanometer scale in the range of 1-100nm (Salamanca-Buentello *et al.*, 2005). The development of nanotechnology have increased dramatically over the decades and its economic potential has grown tremendously (Mody *et al.*, 2010). Therefore, governmental R&D decision makers are setting up new nanotechnology specific programs intending in putting their respective countries in a favorable position for the future. At the same time, government has given considerable funding to various industry sectors in order to challenge this rapid development of nanotechnology (Campañó & Hullmann, 2002).

In recent years, magnetic nanoparticles have been widely employed in medical diagnostics and treatments (Mornet *et al.*, 2004), waste water treatments (Zhong *et al.*, 2006; Xu *et al.*, 2012), catalyst support (Stevens *et al.* 2005), information storage (Chatterjee *et al.*, 2014; Frey *et al.*, 2009) and genetic engineering (Josephson *et al.*, 1999). They have been a focus of interest due to their interesting and practically relevant properties (Khomutov & Koksharov, 2009). Among various types of magnetic nanoparticles, superparamagnetic iron oxide nanoparticles are one of the promising platforms (Zhou *et al.*, 2015) due to their high field irreversibility, high saturation magnetization, high magnetic susceptibility and low toxicity (Akbarzadeh *et al.*, 2012).

A superparamagnetic iron oxide nanoparticle such as nanoparticles of maghemite (γ-Fe_2O_3) offers attractive magnetic properties in many areas such as biomedical (Islam *et al.*, 2012), recording, memory devices, magnetic resonance imaging, drug delivery (Dao *et al.*, 2008) and cell targeting (Sahoo *et al.*, 2010).

Maghemite is known to have unique properties in its nanometer size. However, the most critical problem of maghemite is their tendency to agglomerate. Most of their unique properties can no longer be maintained once the particle start to agglomerate to micron size. Thus, much effort has been made to overcome the agglomeration and chemical destruction problem associated with maghemite nanoparticles (Kluchova *et al.*, 2009). Some methods that have been suggested to overcome these challenges are the use of surfactant or attaching any compatible functional groups to the nanoparticles (Sotiriou *et al.*, 2013). However, with the presence of surfactant, some superior properties need to be compromised.

Various attempts have been made to prepare and functionalise superparamagnetic maghemite nanoparticles such as co-precipitation (Massart, 1981; Wu & Gao, 2012; Lee *et al.*, 2004), hydrothermal synthesis (Islam *et al.*, 2012), micro emulsion (Ang & Yaacob, 2007), sol gel (Tural *et al.*, 2008), polyol thermolysis and high temperature reduction of metal salts, photolysis, sonolysis, multisynthesis processing, and electrochemical (Mody *et al.*, 2010). Yet, exploring the single crystal or monodisoersity of maghemite nanoparticles are still on going.

In this research, pure maghemite nanoparticles without any modification were synthesized using Massart's procedure and the effect of varying ferric nitrate concentrations on the properties of the nanoparticles were investigated. Nitrate or nitrite appears to be promising oxidizing inhibitors for steel and it is relatively low cost, not to forget its ability to increase the potential at the surface of the nanoparticle (Lee *et al.*, 2012). It is known that small size of nanoparticles will tend to agglomerate because of the high surface energy. Many attempts have been made to reduce the agglomeration. However, adding surfactant to reduce the agglomeration might abolish some of the remarkable properties of maghemite nanoparticles. Hence, this process is predicted to reduce agglomeration and promoting monodispersity. Oxidizers can cause passivation of metals by initially reacting with metal resulting in high valance of oxide surface and remain stable at the metal surface, creating a layer that acts as a barrier to further reaction with the metal surface (Ritter *et al.*, 2003).

As the developments of nanotechnology continue to advance, the evolution of electrical device has improved the performance and reduced the chip or system size (Ieong *et al.*, 2004). This aggressive miniaturization of devices has led to the reduction of MOS (metal-oxide-semiconductor) dimension.

MOS structure consists of two conductive regions known as “source” and “drain”. These regions are separated by a semi-conducting channel with associated length and width. A layer of insulating oxide is placed over the channel (Sah, 2005). The ratio of channel width to length is important in determining the performance of the MOS. Over the past 40 years, SiO_2 has been the main material used as insulating oxide of MOS (Osburn & Huff, 2002) due to the good quality of interface and SiO_2 was easy to grow on silicon substrate. However, the scaling of semiconductor capacitor has led to a decrease in thickness of SiO_2 layer (Oswal, 2014). Thus, SiO_2 layer will get so thin and eventually cause substantial leakage through the gate oxide and into the channel (Ieong *et al.*, 2004). The scaling of power device has led to a problem in using SiO_2 in MOS capacitor.

Therefore, researchers are developing new materials with high dielectric current to replace SiO_2. Few materials under consideration to replace SiO_2 include Hafnium Silicate, Hafnium Oxide (Jung *et al.,* 2006), Zirconium silicate and zirconium dioxide (Wilk *et al.*, 2000), iron oxide (Miller *et al.*, 2004) and Samarium Oxide (Goh, 2015). These materials are under consideration due to their excellent electrical properties and high thermal stability in contact with silicon substrate. Maghemite nanoparticles are known to have good advantages in the magnetic application due to its superparamagnetic behaviour it has high dielectric constant value which is 14.2. This value is known to be much higher than SiO_2 which is 3.9. Previously, only few studies focused on maghemite nanoparticle thin film deposited on silicon substrate. Therefore, by exploring the unique properties and behavior of maghemite nanoparticle thin film, it is hoped that some positive result regarding the electrical behavior can be found.

Hence, in this study, pure maghemite nanoparticles were synthesized by varying the parameter of ferric nitrate to investigate the size, stability and magnetic properties of the as-synthesized maghemite. The smallest size with highest solution stability of the as-synthesized maghemite nanoparticles were chosen to be deposited on the silicon substrate using spin coater. Different annealing temperature of the samples (600°C. 700°C, 800°C and 900°C) were used as a parameter to investigate the electrical properties yield by the samples.

1.2 Objectives

There are three objectives in this study:

1. To synthesis maghemite nanoparticles within the size range of 10 nm using Massart’s procedure
2. To investigate the effect of ferric nitrate concentration on the particle size, stability and magnetization of maghemite nanoparticles.
3. To investigate the physical and electrical properties of maghemite nanoparticles deposited on silicon substrate.

There are two aims of this study. The first one is to find the optimum concentration of ferric nitrate used to produce the smallest size of maghemite nanoparticles with high stability and high magnetization to be deposited on silicon substrate.

The second one is to find the optimum annealing temperature of the as-deposited maghemite nanoparticles on silicon substrate to produce high electrical field and low leakage current device.

1.3 Scope of Study

In this study, the scope of the study can be divided into three major stages.

Stage 1: Synthesis of maghemite nanoparticles (γ-Fe_2O_3) using Massart's procedure. The effect of varying the parameter of ferric nitrate (0.1 M, 0.3 M, 0.5 M, 0.7 M and 1.0 M) will be investigated. In this stage, five samples were produced.

This stage was inclusive of the optimization process where all samples underwent few characterization tests such as XRD, Raman analysis, BET, Zetasizer/Zetapotential, TEM, AGM, and TGA and the smallest size of maghemite nanoparticles with high magnetization saturation and solution stability will be chosen for the next step.

Stage 2: Producing MOS capacitor by deposition of maghemite nanoparticles (γ-Fe_2O_3) on silicon substrate using spin coater.

In this stage, the annealing temperature will be varied. Four different annealing temperatures were studied, which were : 600°C, 700°C, 800°C and 900°C. The annealed silicon substrate will undergo few characterization tests such as XRD, Raman analysis and AFM to investigate the phase changes, thickness of the thin film as well as the distribution of the nanoparticles on the silicon substrate.

Stage 3: The effect on different annealing temperature on the electrical behaviour of the produced MOS will be investigated.

In this chapter, AFM analysis and BPW-800 8" probe station along with Keithley 4200 semiconductor characterization system (SCS) was used to conduct the current–voltage (I–V) measurements.

1.4 Thesis Outline

Chapter 1 explained the overview of this study. The advantage and disadvantage as well as the synthesizing method of maghemite nanoparticles from other researchers were briefly mentioned in this chapter. Besides that, the problem of using the current oxide layer and the reason to explore new high dielectric current material was also briefly discussed.

Chapter 2 discussed the properties and magnetic behaviour of maghemite nanoparticles. Besides that, processing methods used to produce maghemite nanoparticles, comparison of processing methods and noble findings from previous researchers on maghemite nanoparticles were also discussed. The structure of MOS, deposition methods, and limitation of SiO_2 as well as the advantage of maghemite nanoparticles as high-k material candidate on replacing SiO_2 were included in this chapter.

Chapter 3 described the experimental procedures for the synthesis of maghemite nanoparticles and the deposition of the maghemite nanoparticles on silicon substrate. In this chapter, all characterization analysis procedure were also included.

Results and interpretation of data are discussed in Chapter 4 and the conclusions of the findings were mentioned in Chapter 5.

CHAPTER 2: LITERATURE REVIEW

2.1 Iron Oxide

Iron Oxide is a chemical compound that composed of Fe and O where it is allied together by chemical bonds. Iron oxide is known to be the standard compound that is widespread in nature and readily synthesized in the laboratory. It is mostly occur in soil or chemical deposits in rocks or mountains. One of the most common and well-known iron oxides is rust. Besides, iron oxide is one of the most prolific and commonly occurring mineral substances on Earth. The greatest concentrations of iron oxide tend to be in the United States, India, Australia, China, Brazil, and Russia. The consequence of this widespread distribution is due to the interest of many scientists from various fields. Though there are different type of iron oxide exists, only some of the iron oxides play a major role in certain application. Some of the applications of iron oxide are bank cards and digital scanning devices, cosmetics, and it is also used to create pigments. There are 16 types of iron oxide including the oxide hydroxides, hydroxides and oxides (Schwertmann & Cornell, 2008). Common types of iron oxides and their properties are tabulated in Table 2.1.

Table 2.1: Iron oxide and their properties

Types of Iron Oxide	Description
Geothite 	**Chemical Formula:** α-FeO(OH) **Crystal Symmetry:** Orthorombic **Colour:** Nuances from black, brown to brownish yellow. **Density:** 4.3 g/cm^3
Lepidocrite 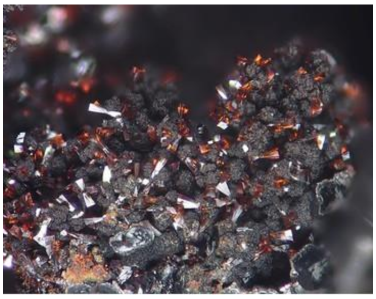	**Chemical Formula:** γ- FeO(OH) **Crystal Symmetry:** orthorhombic **Colour:** dark red to reddish-brown **Density**: 3.3 to 4.3 g/cm^3
Akaganite 	**Chemical Formula:** β-FeO(OH,Cl) **Crystal Symmetry:** Monoclinic **Colour:** Brownish yellow **Density:** 3.52 g/cm^3
Schwertmannite  	**Chemical Formula:** $Fe_8O_8(OH)_6(SO_4)\cdot nH_2O$ **Crystal Symmetry:** Opaquetetragonal **Colour:** Brownish yellow. **Density:** 3.88 g/cm

Table 2.1 continued

Ferroxyhyte 	**Chemical Formula:** FeO(OH) **Crystal Symmetry:** Hexagonal **Colour:** Brown **Density:** 4.2 g/cm^3
Ferrihydrite 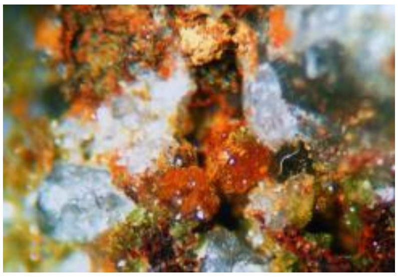	**Chemical Formula:** $Fe_{10}O_{14}(OH)_2$ **Crystal Symmetry:** Trigonal **Colour:** Dark brown, yellow-brown **Density:** 3.8 g/cm^3
Bernalite 	**Chemical Formula:** $Fe(OH)_3 \cdot nH_2O$ **Crystal Symmetry:** Orthorhombic **Colour:** Dark bottle-green to yellow-green **Density:** 3.32 g/cm^3
Magnetite 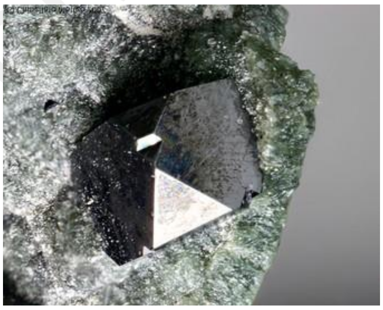	**Chemical Formula:** Fe_2O_4 **Crystal Symmetry:** Isometric **Colour:** Greyish black or iron black **Density:** 5.175 g/cm^3

Table 2.1 continued

Hematite 	**Chemical Formula**: α-Fe_2O_3 **Crystal Symmetry**: Trigonal **Colour**: Steel-grey to black **Density**: 5.26 g/cm^3
Wustite 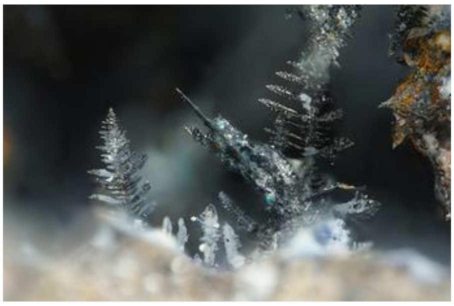	**Chemical Formula**: FeO **Crystal Symmetry**: Isometric-hexoctahedral **Colour**: Gray **Density**: 5.88 g/cm^3
Maghemite 	**Chemical Formula**: γ-Fe_2O_3 **Crystal Symmetry**: Isometric **Colour**: Dark brown **Density**: 4.9 g/cm^3

2.1.1 Maghemite Nanoparticles

Maghemite is a red-brown ferromagnetic. It has cubic spinel structure (Schwertmann & Cornell, 2008). Maghemite (γ-Fe_2O_3) represents an important class of magnetic transition metal oxide materials in which oxygen atoms form a close-packed fcc structure. Moreover, maghemite is an ideal candidate for fabrication of luminescent and magnetic dual functional nanocomposites due to its excellent transparent properties (Wu *et al.*, 2010). Maghemite is known to be the second most stable polymorph of iron oxide. In contrast with the magnetization of hematite (α- Fe_2O_3), which is known to be antiferromagnetic, maghemite exhibits ferromagnetic ordering with a net magnetic moment (2.5 μB per formula unit) and high Néel temperature (~950 K). It is also chemically stable and low cost which led to its wide application in various field (Grau-Crespo *et al.*, 2010).

2.1.2 Processing Methods

As maghemite assembling its attention in this 21st century due to its various application in various field, the synthesis in nano range has also been an active and challenging in the area of research (Mohapatra & Anand, 2010). It was reported that meticulous selection of pH, concentration of the reactant, temperature, method of stirring, precipitation process and rate of oxidation can have a significant effect on the particle size, magnetization value as well as biodistribution (Mohapatra & Anand, 2010). The experiment of using alkaline precipitation of $FeCl_2$ and $FeCl_3$ with controlled precipitation method of superparamagnetic iron oxide particle was firstly done by Massart in 1981 (Massart, 1981). Tartaj *et al.* (2006) reported that the pH and the ionic strength of the solution plays a great role in determining the size and size distribution width of the particle. As the pH increased, the particle size and the size distribution width will become smaller. This is because the parameters are in charge of determining the chemical composition of the crystal surface and consequently the electrostatic surface charge of the particle (Mohapatra & Anand, 2010). With the list of the techniques used to synthesis iron oxide, a lot of studies have been done, and a lot of parameters have been investigated (Lee *et al.*, 2004; Sreeja & Joy, 2007; Ang & Yaacob, 2007; Tural *et al.*, 2008; Islam *et al.*, 2012; Wu & Gao, 2012). By focusing on the chemical precipitation method, previous studies have reported that it is perhaps the simplest way of all the methods listed. Not only simplest, but also the most capable technique in obtaining generous amount of iron oxide particle. α-Fe_2O_3(hematite), γ-Fe_2O_3(maghemite) and Fe_3O_4(magnetite) are ordinarily prepared by addition of alkaline to iron salt solution and keeping the suspension for ageing (Mohapatra & Anand, 2010). The types of salt used will leave a significant impact in obtaining the size, shape and the composition of the magnetic nanoparticles. Examples of salts are chlorides, sulfates, nitrates, and etc (Kusumoto *et al.*, 2002). Previous studies also stated that this technique might have its drawback as well. The limitation of this chemical precipitation technique is that the only factors that are controlling the growth of crystal is its kinetic factor. Therefore, the control of particle size distribution for the particle is limited (Mohapatra & Anand, 2010). Another study also has reported that critical difficulty of this method is that they tend to form aggregate and grow to minimize the overall surface free energy (Gupta & Gupta, 2005).

2.1.2.1 Comparison of Methods Used to Synthesis Maghemite

As mentioned in the previous section, there are several methods used to synthesis maghemite.

Islam *et al.* (2012) reported a novel synthesis of magnetic materials (Fe_3O_4, γ-Fe_2O_3 and α-Fe_2O_3) nanoparticles using modified hydrothermal method. In their research, a typical synthesis of magnetite (Fe_3O_4) nanoparticles were carried out by modifying the reduction reactions between $FeCl_2$ and ethyleneglycol. Maghemite and hematite was formed by oxidizing the as-synthesis magnetite nanoparticles at 250°C for 8 hours in the presence of oxygen and at 500°C for 3 hours in the presence of Argon gas respectively. The results showed that the nanoparticles has high purity and crystalinity. The nanoparticles was in unique necked structure with a particle size range of 50-60 nm. The magnetic measurements on all kinds nanoparticles indicated that the particles were superparamagnetic at room temperature and showed excellent magnetization values.

Zhou *et al.* (2008) reported a transition of rod-like $FeC_2O_4.2H_2O$ to maghemite, hematite and magnetite nanorods through controlled thermal decomposition. The procedure were carried out by heating the as-prepared $FeC_2O_4.2H_2O$ to 400 °C for 2 hours at the heating rate of 2 °C min^{-1} under nitrogen atmosphere to produce maghemite and in air, to produce hematite, with the other conditions remains the same. In order to produce magnetite, 10 mg of as-prepared $FeC_2O_4.2H_2O$ was sealed in a quart cube with 4 ml of air and the tube was heated tp 400 °c for 2 hours, with heating rate of 2 °C min^{-1}. They reported that the final products of their research composed of fine particles with different crystal orientations. The magnetic measurement showed that the magnetic parameters were relatively higher than the corresponding bulk materials, nanoparticles and other similar nanoraods due to the interactions of subparticles in the rods and shape anisotopies.

Besides that, Ang and Yaakob (2007) reported a successful magnetic iron oxide produced at room temperature via water in oil emulsion method. It was reported that the samples produced were highly crystalline and spherical in shape with the average mean physical size of less than 10 nm. The samples were also reported to have high saturation magnetization values.

Furthermore, Lee *et al.* (2004) reported a chemical co-precipitation technique using the pipette drop method and piezoelectric nozzle method. They reported that the size distribution of the as-prepared maghemite nanoparticles using nozzle method were smaller compared to the typical pipette drop which were 3 to 5 nm and 5 to 8 nm respectively. The magnetization measurement also showed a typical superparamagnetic behaviour with blocking temperature of 75 K and 120 K for the nanoparticles prepared by piezoelectric method and pipette drop respectively.

On the other hand, Wu and Gao (2012) also reported almost the same method to produce pure maghemite (γ-Fe_2O_3) nanoparticles. Wu and Gao (2012) reported to produce a pure maghemite (γ-Fe_2O_3) nanoparticles by co-precipitation method using urea and ammonia as precipitation agent for ferrous and ferric ions at ambient temperature. The samples produced showed a capsule-like tubular in shape with high purity and composition of maghemite nanoparticles. The surface area of the samples also showed a little or almost no micropores. Besides that, the magnetic measurement of the nanoparticles showed a high magnetic properties.

Xu *et al.* (2007) have successfully synthesize iron oxide using sol gel method combined with annealing under vacuum at 200-400 °C. The results showed that different size of iron oxide nanoparticles can be obtained by varying the annealing temperature. The saturation magnetization value and coercivity value also increase as the nanoparticle size increase.

2.1.2.2 Massart's procedure

Massart's procedure or co-precipitation method is considered as the simplest and the best way among other methods. Co-precipitation method is a method of synthesizing Fe_3O_4 which is easier and the success rate is from 96 to 99.9% (Loekitowati Hariani *et al.*, 2013). This method was conducted by mixing two ferrofluid that is Fe^{3+} and Fe^{2+} together at stoichiometric ratio of 2:1 respectively. The solution was then added to the excessive amount of Ammonium Hydroxide to form an instantaneous black precipitate of Fe_3O_4. The solution was left to sediment and the clear supernatant was removed. The precipitate obtained was then washed with deionized water for several times. The washed precipitate was then stirred in a nitric acid solution to transform the Fe_3O_4 into γ-Fe_2O_3. Centrifuge is required to isolate the particle. After that, the precipitate is mixed in the ferric nitrate solution at 90˚C so that complete oxidization of γ-Fe_2O_3 was obtained. The particle is then isolated again and dispersed in deionized water around $pH \approx 2.5$. To obtain a dry specimen, the precipitate should be dried in an oven.

2.1.2.3 Ferric Nitrate

Ferric nitrate is a chemical compound with formula of $Fe(NO_3)_3$. However, it is commonly found in its nanohydrate form, $Fe(NO_3)_3.9H_2O$ because of its deliquescent behaviour. Ferric nitrate nanohydrate, $Fe(NO_3)_3.9H_2O$ is a violet crystalline solid and it is a strong oxidizing agent. The structure of ferric nitrate is shown in Figure 2.1.

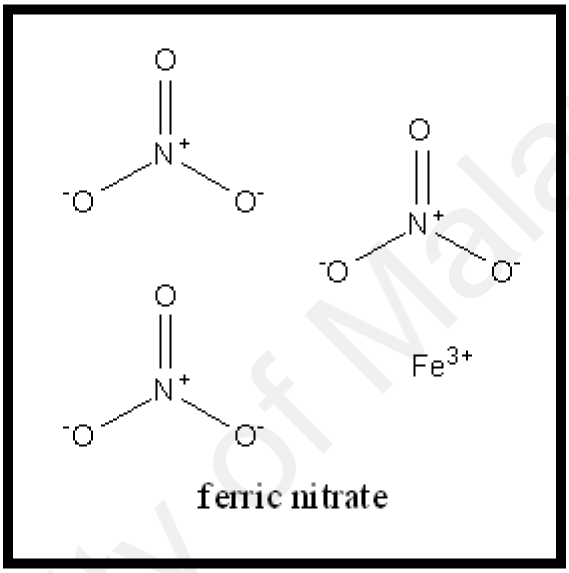

Figure 2.1: Structure of ferric nitrate

There are several applications of ferric nitrate nanohydrate such as in laboratory, it can be used as a catalyst to synthesize sodium amide. Other than that, certain clay impregnated with ferric nitrate has been shown to be a useful oxidant in organic synthesis. In industrial, ferric nitrate solutions are used to etch silver and silver alloys.

Ferric nitrate is usually stable. They are usually used as supported reagents because of their remarkable ease of handling and use. Ferric nitrate has been used to support various inorganic products as an oxidizing reagent for transformation (Lou *et al.*, 2006*)*. The advantage of using ferric nitrate as supported reagents is that good selectivity under mild reaction conditions can be achieved. Besides, it is also easy to isolate the product. Another advantage is the reagent willfully binds to a solid support. This is essential for oxidation reactions so that over oxidation reaction can be minimized (Lou *et al.,* 2006).

In the formation of silver halide, high concentration of KBr will yield to a larger grain. However, if ferric nitrate bleach is added, smaller grain can be produced. This is because ferric nitrate is a strong oxidant. Ferric nitrate also works best and the grain growth will reduced in acidic environment (pH ~ 2.35). The experiment conducted also indicated that ferric nitrate bleach gives the smallest halogenated grains with narrow grain-size distribution (Bjelkhagen, 2013).

2.1.3 Magnetism

Magnetism is a phenomenon which is related to the motion of electric charges. For instance, the electric current in a conductor or changed particles moving through spaces or the motion of an electron in atomic orbit. Other than that, it can also relate to elementary particles such as electron which have a property called spin.

All matter is influenced in varying degrees by the presence of a magnetic field. Magnetism is described best by the field generated by a moving electric charge, and the building block of magnetism is the magnetic dipole thus formed. The simplest magnet, therefore, is an electron with its intrinsic spin. Similarly, the orbital motion of an electron around its nucleus also contributes to the magnetic behavior of materials.

All matter exhibits magnetic properties to some degree. When placed in an inhomogeneous field, matter is either attracted or repelled in the direction of the gradient of the field. This property is described by the magnetic susceptibility of the matter and depends on the degree of magnetization of the matter in the field. Magnetization depends on the size of the dipole moments of the atoms in a substance and the degree to which the dipole moments are aligned on each other. Certain materials, such as iron, exhibit unyielding magnetic properties because of the alignment of the magnetic moments of their atoms within certain small regions called domains. Under normal conditions, the various domains have fields that cancel, but they can be aligned with each other to produce enormous magnetic fields. Figure 2.2 shows a periodic table showing the elements and the types of magnetism at room temperature:

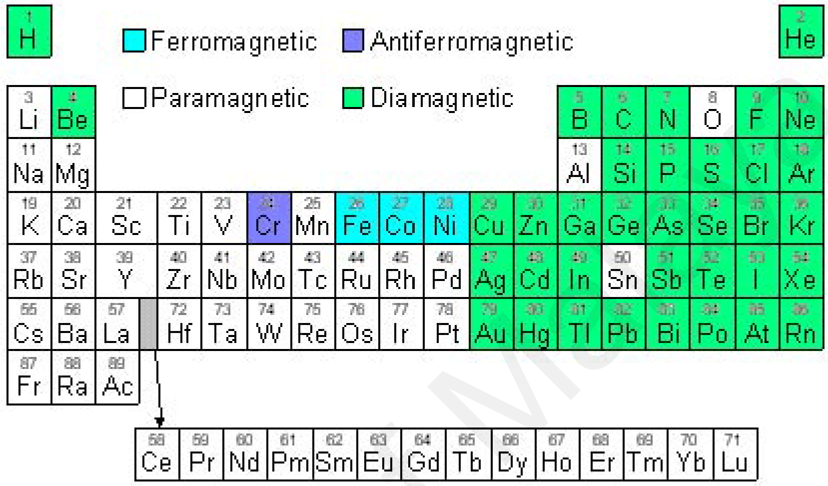

Figure 2.2: Periodic table of elements (Magnetism, n.d.)

There are various advantages of magnetic material. Nowadays, magnetic materials are necessary for many engineering designs, particularly in the area of electrical engineering. Magnetism is dipolar in nature, and no magnetic monopole has ever been discovered until today. There are exactly two magnetic poles of a magnetic field which are separated by a definite distance (Smith & Hashemi, 2006). Mattis (1981) reported that magnetism was first discovered by the ancient Greeks and used by the Chinese to create a “south-pointing” compass. There are many general principles of magnetic behavior have been well established. Some of the principles are:

1. Diamagnetism
2. Paramagnetism
3. Ferromagnetism
4. Antiferromagnetism
5. Ferrimagnetism
6. Superparamagnetism

Iron is known to have a ferromagnetic behaviour as shown in the periodic table in Figure 2.2. The term ferromagnetism is used to characterize a strong magnetic response. The origin of this behaviour is because of the presence of a spontaneous magnetization that is produced by a parallel alignment of spins (Chikazumi & Graham, 1997). Ferromagnetism is a magnetic type that exhibits substantial effect. The magnetization produced is sometimes greater than the applied field. The magnetization effect not only larger than the applied field but also bigger than both diamagnetism and paramagnetism (Chakraborty, 2012). Ferromagnetism is dependent on temperature. It will transform into paramagnetism above the Curie temperature.

Thus, this makes ferromagnetic the most desired magnetism due to the advantages that it provides and thus attracts great deals of interest in it. That is why maghemite nanoparticle has been getting spectacular attraction by the whole world, and people keep on researching about maghemite nanoparticle. Not only providing the versatility of obtaining the particle, but maghemite also exhibit ferromagnetism which is the most desirable and favourable types of magnetism among all. This is because, when a ferromagnetic material is magnetized in one direction, it will not relax back to zero magnetization even after the imposed magnetizing field is removed. Instead, it will drive back to the opposite direction. This condition is known as hysteresis loop and will be disclosed in the next subchapter.

2.1.3.1 Superparamagnetism

Superparamagnetism is magnetism behaviour that occurs in small ferromagnetic or ferrimagnetic nanoparticles. This magnetic behaviour only implies to particles with size of few nanometers to a couple of tenth of nanometers, depending on the material. Additionally, these nanoparticles are single-domain particles. In a simple word, the total magnetic moment of the nanoparticle can be regarded as one giant magnetic moment where it composed of all the individual magnetic moments of the atoms which form the nanoparticle (Pankhurst *et al.*, 2003).

Most applications rely on the magnetic order of the nanoparticles being stable with time. However, with decreasing particle size, the magnetic anisotropy energy per particle responsible for holding the magnetic moment along certain directions becomes comparable to the thermal energy. When this happens, the thermal fluctuations induce random flipping of the magnetic moment with time, and the nanoparticles lose their stable magnetic order and become superparamagnetic (Skumryev *et al.*, 2003).

At such a small size, these nanoparticles do not exhibit multiple domains as found in large magnets. However, on the other hand, they become a single magnetic domain that exhibits high magnetic susceptibility. Thus, on application of a magnetic field, these nanoparticles provide a stronger and more rapid magnetic response compared with bulk magnets with negligible remanence and coercivity (Matsui, 2005; Wajuddin, 2012).

2.1.3.2 Hysteresis Loop

Hysteresis loop can be defined as the traced out of magnetization loop when an alternating field is applied to the material. Hysteresis is named because of the lack of retrace ability of the magnetization curve. This is related to the existence of magnetic domain in the materials. As mentioned earlier, the condition of ferromagnetic can occur once the magnetic field is reoriented and formed energy which is needed to turn them back again. This is shown in Figure 2.3 below:

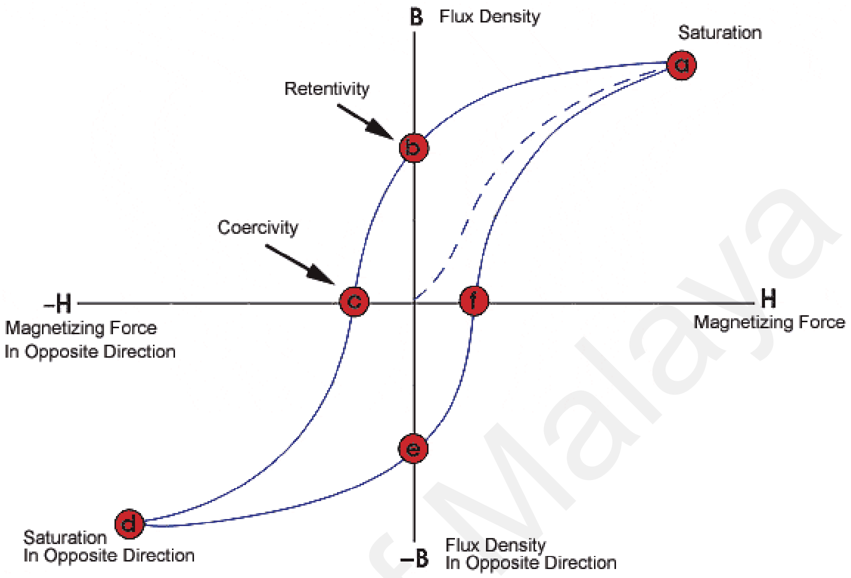

Figure 2.3: Hysteresis loop (Classes of Magnetic Materials, n.d.)

The hysteresis loop is the relationship between the induced magnetic flux density (**B**) and the magnetizing force (**H**). The loop from Figure 2.3 can be achieved by measuring the magnetic flux of a ferromagnetic material while changing the magnetizing force. While increasing the **H** value, a demagnetized ferromagnetic material will follow the dashed line until it reached magnetic saturation at point “a”. When **H** value is reduced to zero, the curve will move from point “a” to “b”. Point “b” can be referred as the point of retentivity as there is remanence level of magnetism in the material since the magnetization is already zero. As the magnetization force reversed, the curve moves to point of coercivity, “c” where the flux has been reduced to zero. Coercivity force is the force required to remove the residual magnetism from the material. As the magnetization force is increased in the negative direction, the material will become magnetically saturated in the opposite direction at point “d”. As the value of **H** is reduced again to zero, the curve will move to point “e” where the level of residual magnetism is equal to that achieved in the opposite direction. By increasing the **H** value in positive direction, the value of B will be zero. The curve will complete the loop from point “f” to the saturation point.

2.2 MOS Capacitor

Silicon power Metal-Oxide-Semiconductor or better known as MOS is the most commonly used unipolar power capacitor. Besides MOS, there are also other structures such as the junction gate field-effect transistor (JFET) or static induction transistor (SIT) that have been explored. However, they have not been very popular as MOS due to their normally-on behaviour (Baliga, 2010).

Figure 2.4 shows the basic structure of a MOS. MOS is a four terminal device which the terminals are designated as gate, bulk, source and drain. Usually, the p-type doped silicon region is referred as bulk or substrate. It is connected via the bulk contact. Two heavily p-type doped regions is called the source and drain. They are formed in the substrate on either side of the gate. Generally, one cannot differentiate between the source and the drain of an unbiased device as the structure is symmetrical. It can be seen that the gate slightly overlap with the drain and source regions. Channel region is located between the juction of source and drain (Galup-Montoro & Schneider, 2007).

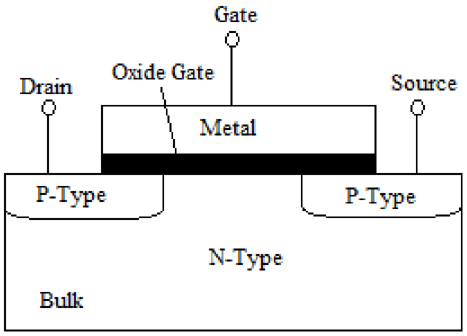

Figure 2.4: Basic structure of MOS capacitor

2.2.1 Oxide Layer

The first semiconductor gates were made of germanium. Germanium is considered to be more efficient due to its small bandgap. Although Si and Ge belong to the same group in the periodic table, they are known to exhibit different surface chemistry regarding adsorption-desorption and also thermal transformation (Asoka-Kumar *et al.*, 1996). Because of the less stable of GeO_2 as compared to SiO_2, SiO_2 has been the important material to be used in MOS as oxide gate for over decades ago due to its high dielectric strength and the interfaces of SiO_2-Si system contain manageable amounts of surface states where it leads to a successful MOS transistor (Kahng, 1976).

2.2.2 Limitatio of SiO_2

Initially, SiO_2 was considered as the material of choice because it was easy to work with on Silicon. Besides, it is easy to grow, and the quality of the interface is good. However, the scaling of semiconductor capacitors has led to a decrease in thickness of the silicon dioxide layer used as gate dielectric. The thickness of the silicon dioxide layer is reduced to increase the gate capacitance, thus increasing the drain current. If the thickness of the gate dielectric decreases below 1.2 nm, the leakage current due to the tunneling increases drastically. There are several of materials with high dielectric constant such as Titanium, Hafnium, and Zirconium oxides are being investigated (Oswal, 2014). Hence, in this study, maghemite nanoparticle was used to investigate the electrical properties of the MOS as it is well known that maghemite nanoparticle, using fast and reversible redox reactions at the surface of active materials, are typical examples of pseudocapacitive materials, which could offer high power density as well as high energy density (Xie *et al.*, 2011).

2.2.3 New high-k material

As electronic devices start to scale down, the complementary MOS capacitor dimension also begun to cut back aggressively (Haensch *et al.*, 2006). Thus, using SiO_2 as oxide gate has become a challenging topic due to its current leakage breakdown as the thickness becoming so thin (Robertson, 2004). Hence, researchers are trying to find new materials to replace SiO_2 in MOS capacitor. There are few materials that have been getting the researchers' attention. (Campbell *et al.*, 1997; Gerritsen *et al.*, 2005; Kadoshima *et al.*; 2003 Nahar *et al.*, 2007) listed the materials of candidate to replace SiO_2 are ZrO_2, HfO_2, Al_2O_3, Ta_2O_5 and Si_3N_4 (Zeng *et al.*, 2014). These materials are listed as high-κ materials due to their dielectric constant more than of SiO_2 which is 3.9. Among all the materials listed above, HfO_2 has become the most promising candidate due to its high dielectric constant of 22-25, high free energy of reaction with Silicon at 727 °C, large bandgap of 5.8 eV and also excellent thermal stability in contact with silicon (Jung *et al.*, 2006). Following the advantages of HfO_2 compare to other materials, Intel have manufactured a 45nm MOSFET using 1.0nm thickness of HfO_2 oxide gate (TU Claustal, 2016).

Table 2.2 shows the dielectric constant value for materials of the candidate to replace SiO_2. As tabulated in Table 2.2, iron oxide has a dielectric constant value of 14.2. This value is three times higher than SiO_2. On the other hand, maghemite nanoparticles are known to have unique characteristic due to its small size. Thus, by taking this into consideration, this study was conducted to explore the compatibility of maghemite nanoparticles as gate oxide layer in MOS capacitor.

Table 2.2: Dielectric constant value for several materials

Materials	Dielectric constant (*K*)
SiN_4	7
ZrO_2	12.5
HfO_2	25
Al_2O_3	9
Ta_2O_5	22
Fe_2O_3	14.2

2.3 Deposition Methods

There are various methods to deposit oxides onto a silicon substrate. Some of the methods are physical vapor deposition (PVD), chemical vapor deposition (CVD) (Maruyama & Arai, 1992), sputtering deposition ion plating and spin coating.

2.3.1 Physical Vapor Deposition (PVD)

PVD is a deposition technique which can be used to produce a thin film with thickness in the range of few nanometers to thousands of nanometers (Mattox, 2010). In the early days of microelectronics, PVD was directly used to evaporate Aluminium to the capacitor to form the conductivity connections. However, as the complexity of Si integrated circuit increased, a wider range of materials are needed to be deposited on the capacitor to fulfill various kinds of demands (Moshfegh, 2004).

There are several advantages of using PVD such as, as corrosion protective coatings, wear resistant coatings, electrically conducting films, decorative coating, mirror coatings, and it can be used to form optical interference coating as well as a permeation barrier films on flexible packaging materials (Moshfegh, 2004). The illustration of PVD techniques is shown in Figure 2.5 below.

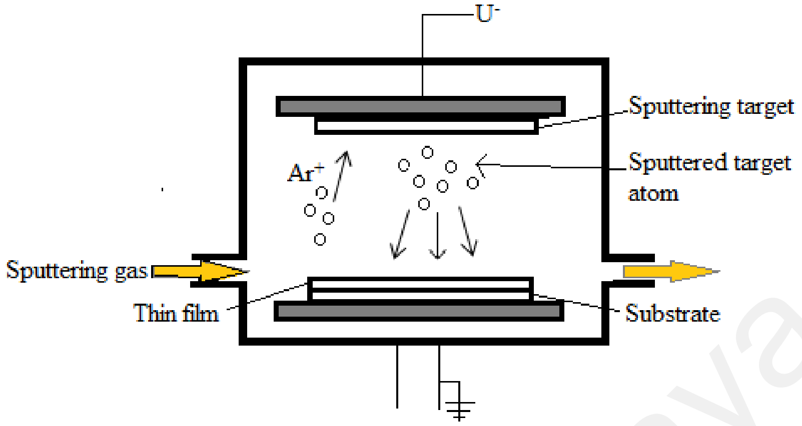

Figure 2.5: PVD process

2.3.2 Chemical Vapor Deposition (CVD)

Identical with PVD, CVD is also widely used in material processing technology. The majority of its applications also are comparable with PVD. The applications involve applying thin-film coatings to surfaces, produce high-purity bulk materials and powders and also to fabricate composites (Park & Sudarshan, 2001).

Even though the function of CVD is almost the same with PVD, there are many advantages of using CVD that makes it preferred as compared to other techniques. The benefits of CVD are that, CVD allow coating a surface with uniform thickness, selective deposition and also low deposition temperature (Hampden-Smith & Kodas, 1995).

However, CVD also has its drawback. The drawbacks are CVD works mostly at temperature 600°C and above. Many substrates are not thermally stable, thus cannot withstand the high temperature. Besides that, using chemical precursors are often hazardous and sometimes extremely toxic (Pierson, 1999). Figure 2.6 shows illustration of CVD technique.

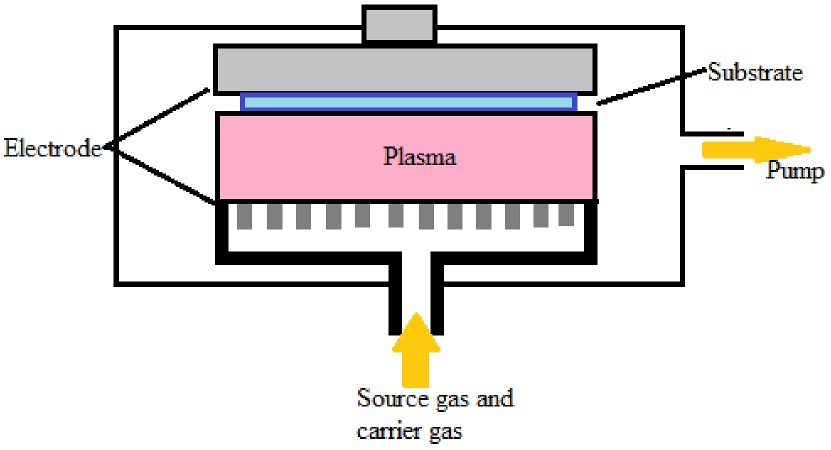

Figure 2.6: CVD process

2.3.3 Sputtering Deposition

Sputter deposition is a method of producing thin film by sputtering. The process is done by ejecting material from a source (target) onto a substrate. Figure 2.7 shows the sputtering gas bombards the target and sputter off the desired material (TU Clausthal, 2016). It is known for surface coating technologies used as decorative coatings, tool coating, and other coating applications.

There are some advantages and disadvantages of sputtering deposition method. Some of the benefits are different types of elements can be sputtered such as alloys and compounds. The sputtering techniques provide a stable and long-lived vaporization source. Besides that, the source and substrate can be located closed together and there is little radiant heat in the deposition process.

However, there are also some disadvantages such that, the sputter rate are low, the distribution is not uniform, the targets are also very expensive and sometimes, the film can be contaminated due to active gas contaminants in the (TU Clausthal, 2016).

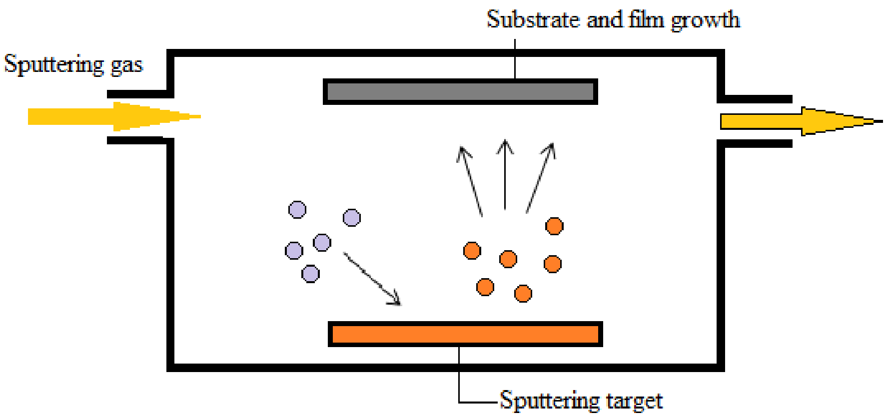

Figure 2.7: Sputtering deposition technique

2.3.4 Ion Plating

Ion plating is a technique of film formation where the substrate is subjected to a flux of energy ions sufficient to cause an appreciable sputtering (Mattox, 1973). The benefits of using ion plating method are its ability to sputter clean surface until the film starts to form. Besides that, it provides a high flux to the surface of the substrate and thus enhancing the diffusion and chemical reaction. Other than that, by introducing a high defect concentration, ion sputtering is able to alter the surface and interfacial structure causing the film and the substrate material to mix with each other and influencing the nucleation and growth of the depositing film. This technique also particularly effective in obtaining good adhesion is some system, Figure 2.8 illustrate the diagram of ion sputtering technique (Mattox, 1973).

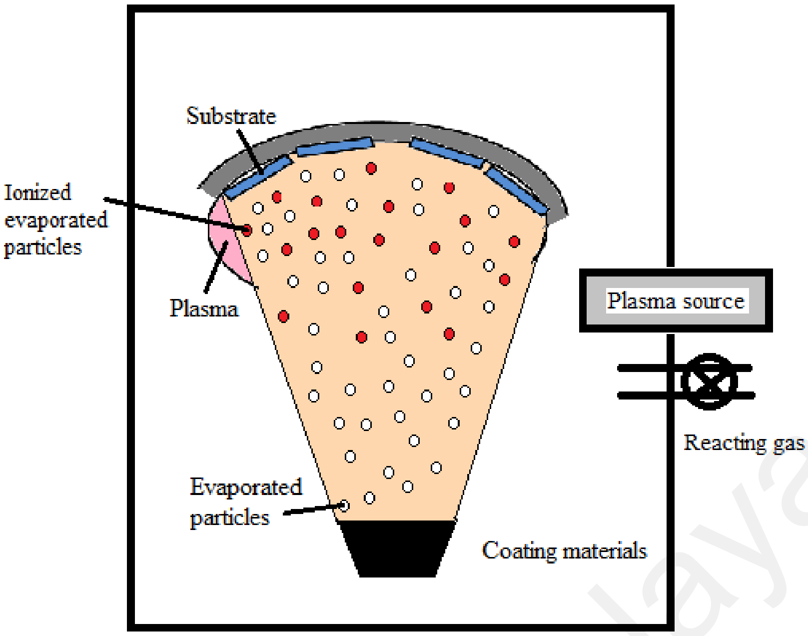

Figure 2.8: Ion plating technique

2.3.5 Spin Coating

Spin coating is a method of forming a thin film that has been used for several decades. It involves a process of depositing a small puddle of fluid on the center of the substrate and spins a high speed. The resin will spread and then, will eventually off from the edge of the substrate leaving a thin material on the surface of the surface. This action is caused by the centripetal acceleration. The nature of the fluid material such as viscosity, percent solids and surface tension will determine the materials' thickness (TU Clausthal, 2016). Figure 2.9 shows the illustration of the spin coating technique.

The favor of spin coating process is the simplicity and low cost. Besides achieving uniform and thin coating, this process also allow the materials to dry at a faster time due to its high spin speed. This will results in the high consistency at both macroscopic and nano length scale.

On the other hand, the drawback of this method are it is time-consuming because it is an inherently batch process. Other than that, in some nanotechnology applications, fast drying time can lead to a lower performance of the device. The material usage is typically very low while the rest was being wasted. However, despite of these drawbacks, spin coat usually used as a starting point in producing a thin and uniform coating (TU Clausthal, 2016).

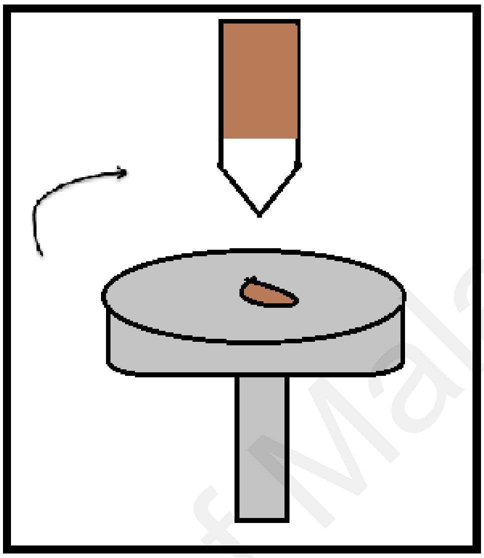

Figure 2.9: Spin coating technique

2.4 Summary

The synthesis of maghemite nanoparticles has been an intensive study over the past few years due to its unique properties. There have been many methods reported by previous researchers to synthesize maghemite nanoparticles. However, controlling the agglomeration of the nanoparticles still remains a challenging subject. Therefore, this study showed the improvement of the agglomeration issues by investigating the optimum concentration of ferric nitrate needed in order to produce the smallest size of the nanoparticles with high stability and high magnetization saturation to be deposited on silicon substrate. MOS device is going through a phase change of the oxide layer material since SiO_2 thickness have reached its limit. Several high-k materials have been investigated to improve the performance of the MOS device. However, there are still no work reported on the unmodified maghemite nanoparticles. Thus, this study reported on the electrical performance of the unmodified maghemite nanoparticles deposited on silicon substrate.

CHAPTER 3: METHODOLOGY

3.1 Materials and Methodology

In this chapter, the materials used, experimental setup and the parameter used to analyze the samples are described.

3.1.1 Raw Materials and Experimental Procedure

This study consisted of two stages. All stages consist of the characterization of the prepared samples. A flowchart of the research methodology is shown in Figure 3.1.

The first stage of this study was the synthesis of maghemite nanoparticles using Massart's procedure. The chemical reagents used in this experiment were ferrous chloride hexahydrate ($FeCl_3.6H_2O$), ferric chloride tetrahydrate ($FeCl_2.4H_2O$), hydrochloric acid (HCl), ammonium hydroxide, nitric acid (HNO_3) and ferric nitrate ($Fe(NO_3)_3.9H_2O$). All of these chemical reagents were manufactured by R&M Chemicals and used without any purification. Water used in this experiment was deionised water.

The second stage of this study involved the deposition of maghemite nanoparticles on silicon substrate using micropipette and spin coater. The first step in this stage was cleaning the silicon substrate. Raw materials used to clean the silicon substrate were ammonium hydroxide (NH_4OH), hydrogen peroxide (H_2O_2), hydrochloric acid (HCl), hydrogen fluoride (HF) and deionized water. All of these chemical reagents used were manufactured by R&M Chemicals.

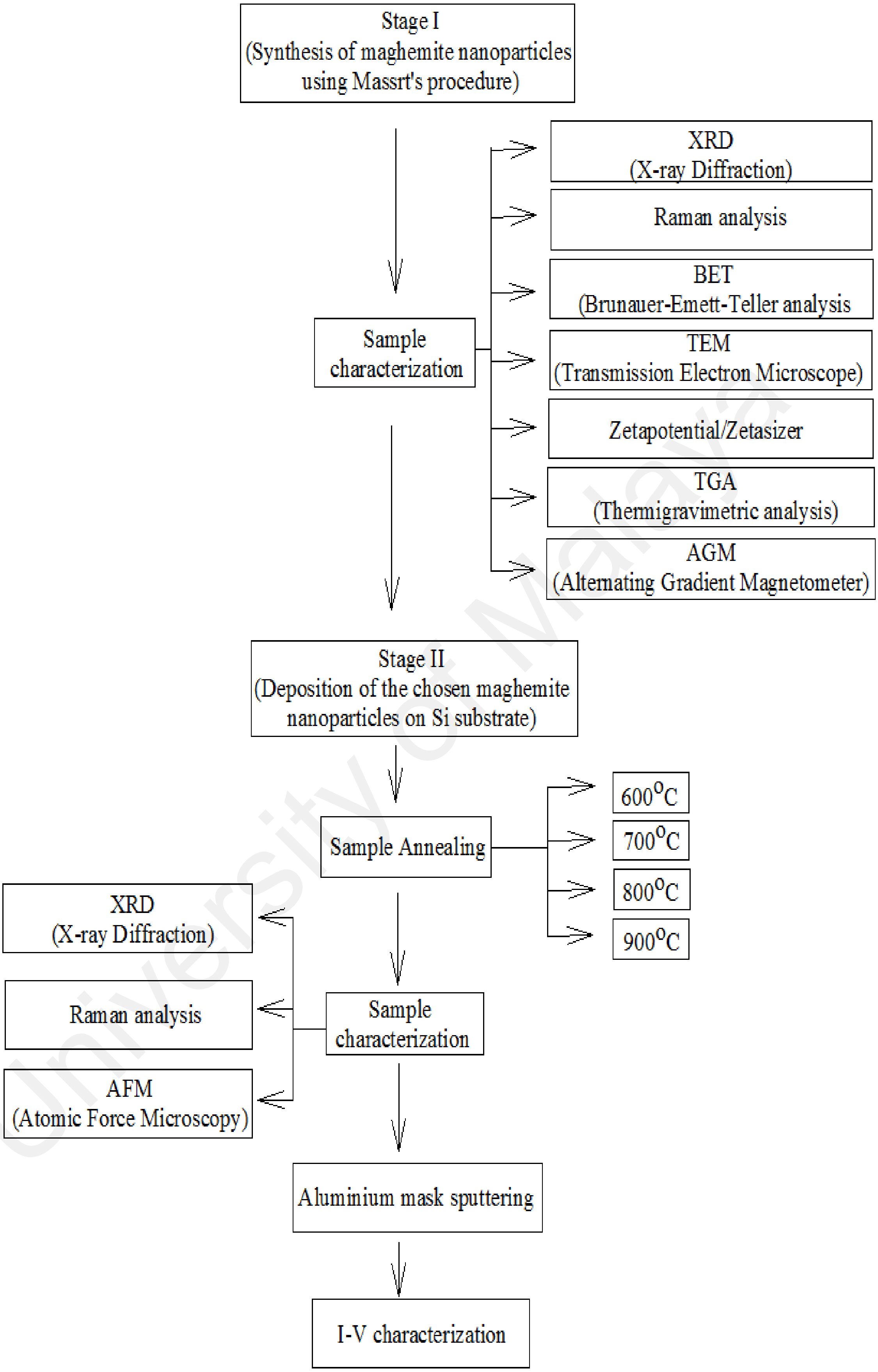

Figure 3.1: Flowchart of the research methodology

3.2 Synthesis of Maghemite Nanoparicles using Massart's Procedure

Maghemite nanoparticles were synthesized using Massart's procedure and the effects of varying the concentration of ferric nitrate were investigated. The procedure is illustrated in Figure 3.2 and the chronology of the process is described as follow:

1. Ferric Chloride ($FeCl_3$) and Ferrous Chloride ($FeCl_2$) was mixed until homogeneous. Few drops of HCl were added to the ferrous chloride to stabilize it.

2. NH_4OH was added to the homogeneous solution of ferric and ferrous chloride solution. Instantaneous black precipitates were formed. This indicated that magnetite precipitates (Fe_3O_4) were obtained.

$$FeCl_2.4H_2O + 2FeCl_3.6H_2O + 8NH_4OH \rightarrow Fe_3O_4 + 4H_2O + 8NH_4Cl \qquad (3.1)$$

3. After the precipitates settled down at the bottom of the beaker, the clear supernatant was removed and the precipitates were washed several times to ensure that excess NH4OH were removed.

4. The particles were then peptized in 1 M of HNO_3 solution with continuously stirring for 10 minutes.

$$2Fe_3O_4 + HNO_3 \rightarrow \gamma\text{-}3Fe_2O_3 + HNO_2 \qquad (3.2)$$

5. The particles were washed again before oxidized with different concentration of $FeNO_3$ solution at 90°C for 30 minutes.

6. The particles were isolated by magnets and dispersed in deionized water at pH~ 2.5 in order to maintain the stability of maghemite nanoparticles.

In this stage, five samples were prepared with different concentration of $Fe(NO_3)_3.9H_2O$ solution while maintaining the ratio of Fe^{3+} and Fe^{2+} at stoichiometrical ratio of 2:1. Table 3.1 tabulated the concentrations used in the experiment.

Table 3.1: Different Concentration of $Fe(NO_3)_3.9H_2O$ solution

Sample	**Conc. of $Fe(NO_3)_3.9H_3O$ (M)**	**Conc. of $FeCl_2$ (M)**	**Conc. of $FeCl_3$ (M)**
G1	0.1	0.1	0.2
G2	0.3	0.1	0.2
G3	0.5	0.1	0.2
G4	0.7	0.1	0.2
G5	1.0	0.1	0.2

Five samples were produced using different $Fe(NO_3)_3.9H_2O$ concentrations: 0.1 M, 0.3 M, 0.5 M, 0.8 M and 1.0 M. The samples were labelled as G1, G2, G3, G4, and G5 respectively. Fe^{3+} : Fe^{2+} molar ratio of 2:1 were remained.

The maghemite nanoparticles obtained were characterized using XRD, Raman, TGA, BET, AGM, TEM, Zetapotential and Zetasizer.

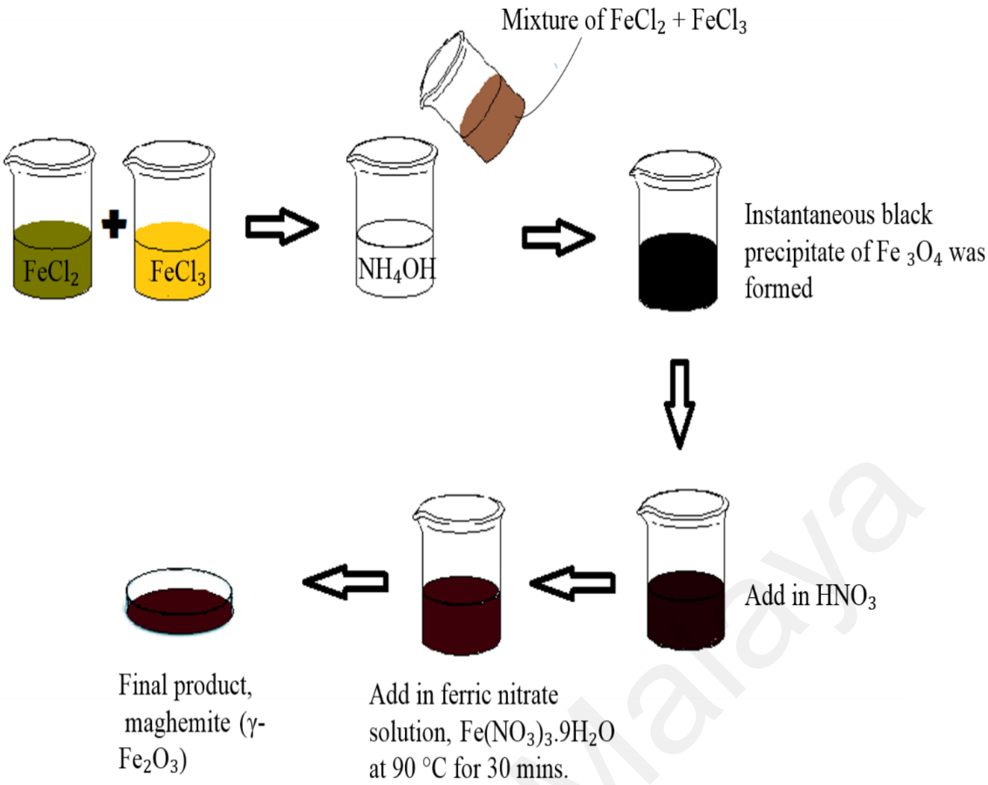

Figure 3.2: Diagram of Massart's procedure

3.3 Development of Maghemite on Silicon Substrate

N-type silicon substrate was cut 1cm × 1cm. The substrate was then cleaned using RCA cleaning step. RCA clean consist of three phases. The first phase was to remove organic contaminants (such as dust particles or grease) from the wafer surface, the second phase was to remove the oxide layer and the third phase was to remove ionic or heavy metal contaminants.

After the cleaning process, the smallest size of maghemite nanoparticles (G3) was chosen to be developed on the silicon substrate using spin coater. 40µl of the suspension was taken using micropipette and was spin coated at 2500 rpm for 1 minute. The sample was then annealed at different temperatures. The procedure of the spin coating is illustrated in Figure 3.3 below and the flowchart is summarized in Figure 3.1.

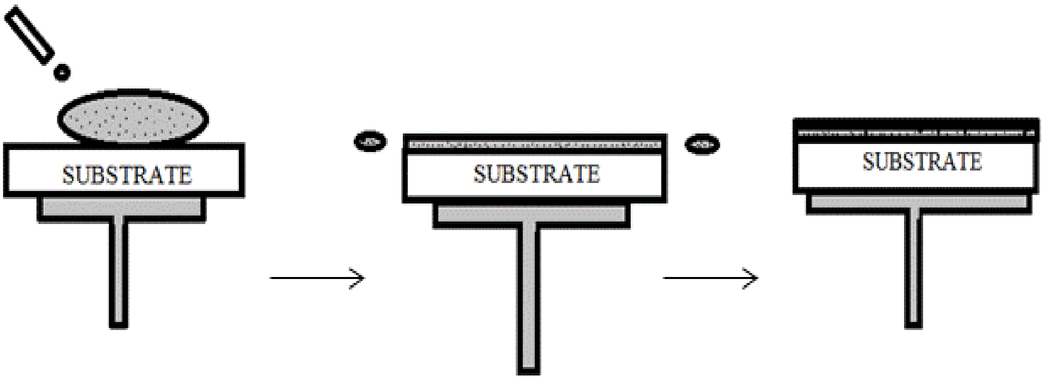

Figure 3.3: Spin coating process

5 samples were produced. The samples were then annealed at 5 different temperature. Table 3.2 shows the different samples with different annealed temperature.

Table 3.2: Different annealed temperature

Samples	Temperatures
1	600°C
2	700°C
3	800°C
4	900°C

The annealed samples was then undergone physical characterization analysis such as X-Ray Diffraction (XRD), Raman analysis, Atomic Force Microscopy (AFM) and Field Emission Scanning Electron Microscopy (FESEM) before sputtered with Aluminium. The sputtered samples was then undergone Current-Voltage (I-V) characteristic curve in order to investigate their electrical properties.

3.4 Characterization Parameter

The crystallographic structure and phase identification of the powder sample was studied through X-ray Diffraction (XRD) model Empyrean manufactured by

PANanalytical Model No. of DY1032. The sample was measured at the scan rate of 0.05 s^{-1} in a range of (20°-80°) for 2θ at radiation of CuK_{α} (wavelength 1.54056 Å).

Raman Spectroscopy (Renishaw) was used to characterize the information about the molecular vibration that was used to identification and quantitation of the sample. The frequency of the instrument was taken from 200 cm^{-1} up to about 1700 cm^{-1}. The laser power used was 0.5 mW for 10 seconds.

BET (Brunauer-Emett-Teller) was used to investigate the surface area of the samples. In this experiment, 0.1 - 0.5 g of sample was filled in a sample tube and degassed at 120°C for 9 hours before measurements are done. This step is to ensure that all air and moisture is removed from the sample. After the degassing process, net weight of the sample can be obtained by measuring the empty sample tube and the weight of the sample tube filled with sample after degassing process. Blank analysis was performed using Helium gas as the measurement gas while nitrogen was used as adsorption gas.

Zetasizer (Malvern Instrument) was used to measure the particle size, zeta potential and molecular weight of the sample. The sample used was in the form of liquid. From this experiment, hydrodynamic size of the particles was obtained and the stability of the sample was measured using zeta potential.

Transmission electron microscope (TEM) manufacture by JEOL model JEM 2100F was used to examine the structure, size and the shape of the sample. Sample preparation was done by spreading one drop of the suspension on a carbon-coated copper grid and dried for several hours. The dried sample was inserted into the chamber and images were captured.

Alternating Gradient Magnetometer (Micromag, model 2900 was used to study the response of magnetic force. The mass of the samples used was approximately 0.3-0.8 mg of powder sample. The nanoparticle powder was weigh and adhered on adhesive tape and placed onto transducer probe by applying some silicon grease. The transducer was then placed on the piezoelectric and measurements were initiated. A gradient field strength alternating from maximum 10 kOe and minimum of -10 kOe is exerted on the sample.

Thermogravimetric Analyser (Mettler Toledo, Model No.: TGA/SDT A851E) was used to study the thermal analysis of the sample. The weight change of the sample was observed after the sample was being heated in a furnace at a heating rate of 10˚/min within a range from ambient temperature to 1000˚C.

Electrical characterization of the as prepared film was investigated by fabricating MOS capacitor test structures with defined square area of 1 cm x 1 cm. 100 nm-thick aluminum (Al) (Kurt J. Lesker, USA, 99.9995 % purity) was sputtered on top of the film using TF 450 physical vapour deposition (PVD) RF sputtering system. BPW-800 8" probe station along with Keithley 4200 semiconductor characterization system (SCS) was used to conduct the current–voltage (I–V) measurements.

Hitachi AFM5000II with scan voltage of ±200 V was used to study the surface morphology of the MOS capacitor.

CHAPTER 4: RESULTS AND DISCUSSION

4.1 Synthesis of γ-Fe_2O_3 nanoparticles

4.1.1 Microstructural Study analysis

Figure 4.1 shows the XRD curve for all samples labelled as G1, G2, G3, G4 and G5. The diffraction patterns collected were from 20° to 80°. It can be seen that all samples exhibit similar pattern and similar peaks. Figure 4.2 shows the cropped data of the XRD curve. The pattern matched with γ-Fe_2O_3 with a strong (311) peak at approximately 35.6° accompanied with the (220), (400), (511) and (440) planes at approximately at 30.4°, 43.4°, 57.5° and 63.0° respectively. These peaks are consistent with the standard structure (JCPDS No. 98-008-7119) for maghemite and (JCPDS No. 001-089-5892) for magnetite. Ferroudj *et al.*, (2013) reported that sharp and relatively well defined peaks are observed at the interplanar spacing of d_{220}, d_{311}, d_{400}, d_{511} and d_{400} which are the characteristic of the crystal structure of maghemite. However, it is well known that from the basis routine of XRD, maghemite and magnetite are difficult to distinguish as they have closely matched XRD pattern (Chaudhari *et al.*, 2011). Therefore, further analysis is needed to prove that the samples are maghemite. From Figure 4.2, at plane (311), (511) and (440), the peaks of sample G5 can be seen to be shifted at a lower angle. This might be because of the difference in the lattice constant. The average lattice parameter was calculated from plane (311), (511) and (440) and presented in Table 4.1.

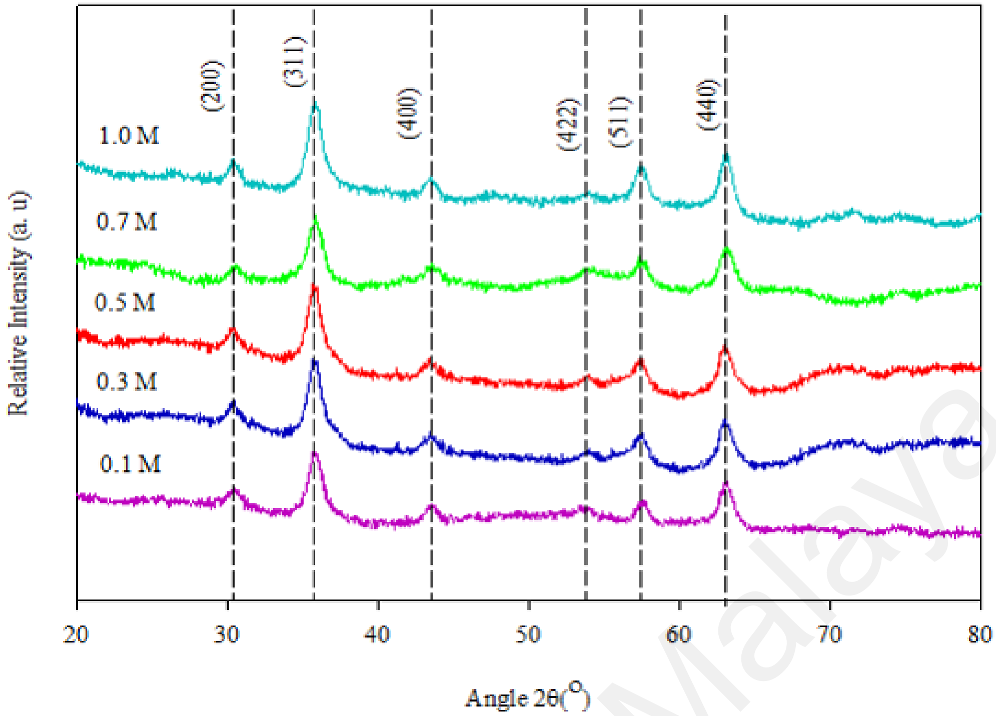

Figure 4.1: XRD curve for all samples

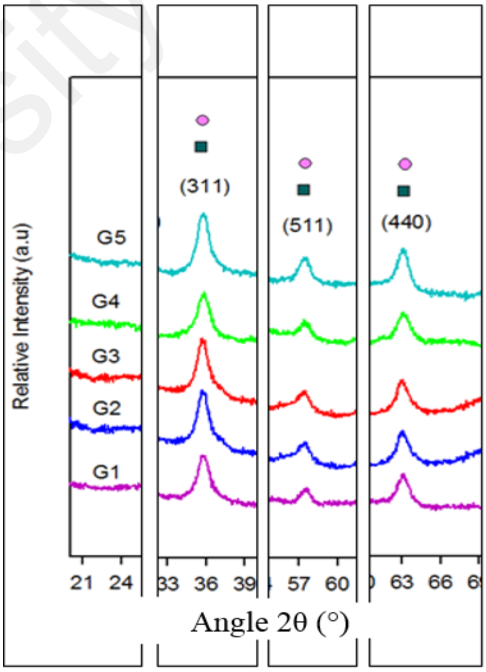

Figure 4.2: XRD curve at defined peaks

The lattice parameter of all samples was calculated from the XRD result using the following equation (Smith & Hashemi, 2006):

$$\boldsymbol{d_{hkl}}\text{:}\ \frac{\boldsymbol{a}}{\sqrt{\boldsymbol{h^2 + k^2 + l^2}}} \tag{4.1}$$

As reported by Vidal-vidal *et al.* (2006) and Ang *et al.* (2014), the difference of lattice parameter between magnetite and maghemite is very small. The lattice parameter of magnetite is 8.38 – 8.39Å while lattice parameter of maghemite is 8.35Å. From Table 4.1, lattice constant for all samples was in the range of 8.33-8.35 Å which belong to maghemite group. Therefore, the result obtained from XRD test strongly affirms that the nanoparticles belong to maghemite. The average crystallite size of the samples was calculated from 3 main peaks at plane (311), (511) and (440) using Sherrer’s equation:

$$D = \frac{0.94\lambda}{\mathrm{B}\cos\theta} \tag{4.2}$$

where *D* is the average crystallite size , λ is the x-ray wavelength, B is the line broadening at half the maximum intensity (FWHM) and θ is the the Bragg angle. The crystallite size calculated was 9.34 nm, 5.09 nm, 3.59 nm, 5.00 nm and 6.41 nm for sample G1, G2, G3, G4 and G5, respectively.

Table 4.1: Lattice parameter and crystallite size for all samples

Sample	Lattice Parameter, a (Å)	Crystallite Size (nm)
G1	8.33	9.34
G2	8.34	5.09
G3	8.33	3.59
G4	8.33	5.00
G5	8.35	6.41

Figure 4.3 shows the comparison graph of crystallite size and average lattice parameter. From the graph, the sizes of the nanoparticles are gradually decreases as the concentration of ferric nitrate increased up to 0.5 M. However, the size of the nanoparticles starts to increase once the ferric nitrate concentration increased further. From this phenomenon, it can be said that each concentration of ferric nitrate has different solubility level. The solubility level will affect the growth and nucleation process during the synthesis process.

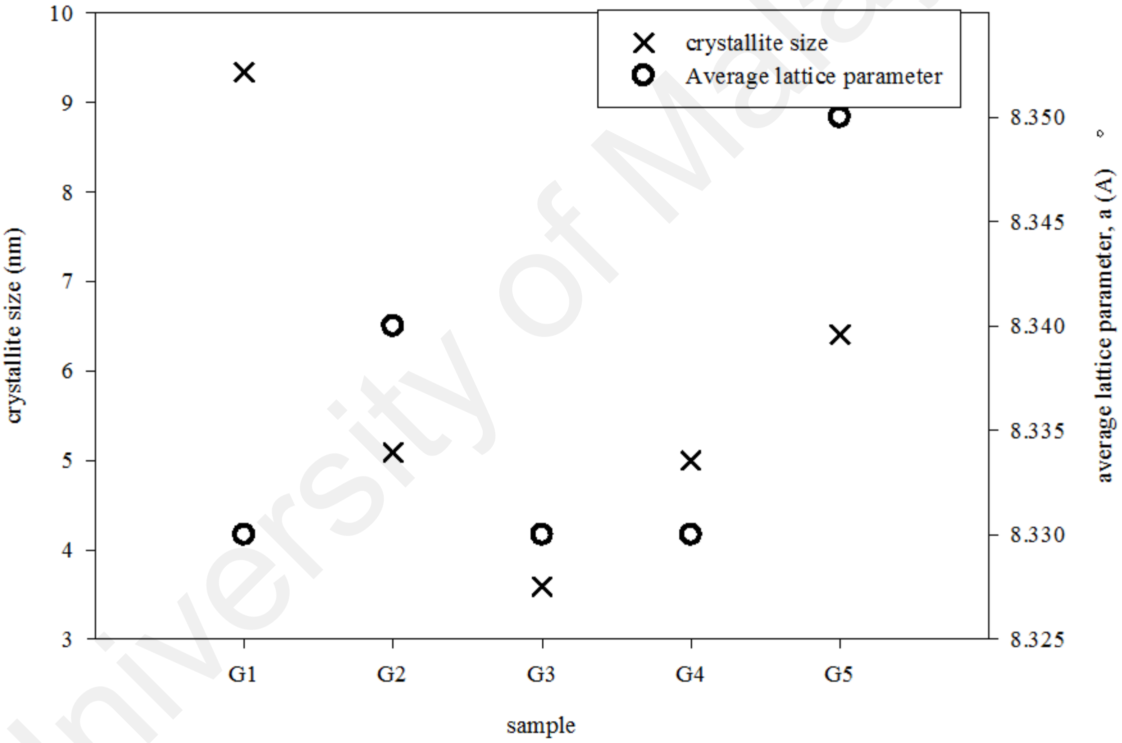

Figure 4.3: Comparison of crystallite size and lattice parameter for all samples

4.1.2 Raman analysis

Raman spectra for sample G1, G2, G3, G4 and G5 are presented in Figure 4.4. From the curve, all samples exhibit almost similar peak with the strongest peak at 720 cm^{-1}, followed by 350 cm^{-1}, 500 cm^{-1} and 1390 cm^{-1}. These four peaks indicated that the particles belong to further confirm and differentiate between magnetite and maghemite nanoparticles (Hanesch, 2009). From the graph obtained, no peak around 670 cm^{-1} can be seen for all samples (Li *et al.*, 2012). This indicated that there is no presence of magnetite in the particles.

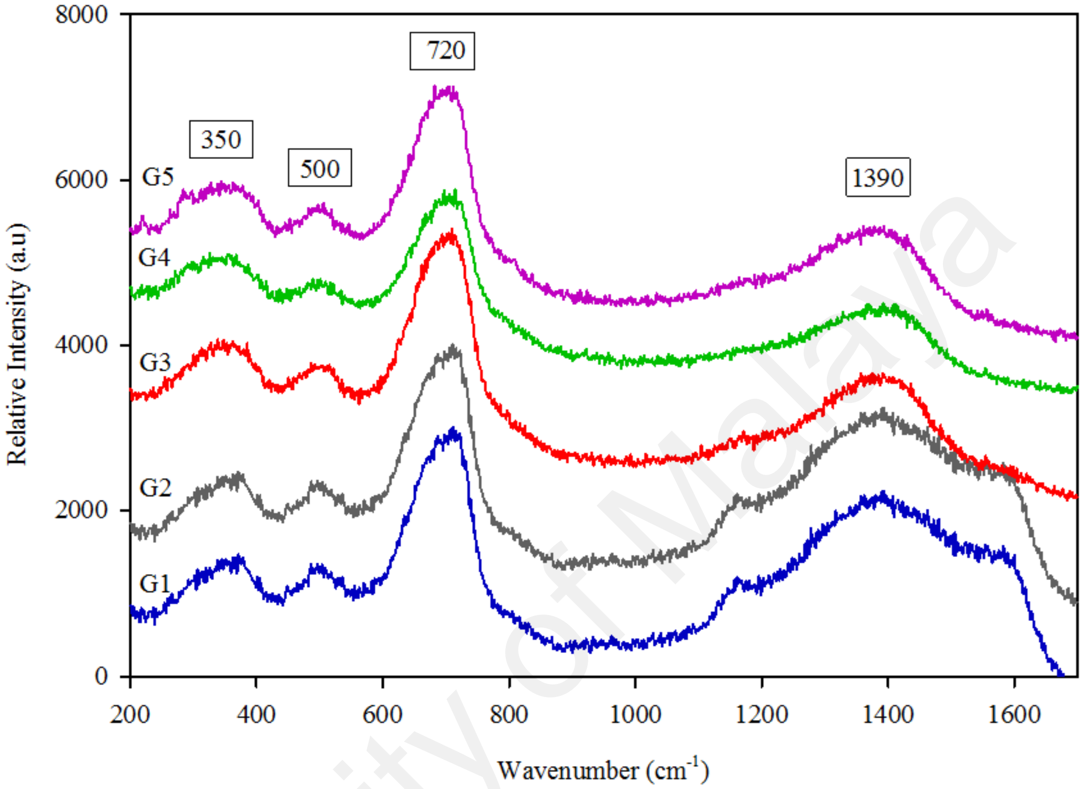

Figure 4.4: Raman curve for all samples

From the peaks, it can be seen that samples G1, G2, and G3 are shifted to the left while sample G4 and G5 are shifted to the right. The shifts to the left indicated that the samples have smaller grain size stress (Chi *et al.*, 2011). Meanwhile, as sample G4 and G5 are shifted to the right, the grain size stresses are bigger.

However, for sample G1 and G2, extra two peaks are found located at approximately around 1150 cm^{-1} and 1600 cm^{-1}. It was reported by Chi *et al.* (2011), the peaks of raman shift that occurs at (1020-1100 cm^{-1}) are due to the detection of “pure” hydroxide (white rust). For peak approximately around 1600, it was reported by Hanesh (2009) that the peak ocuured is independent of the maghemite bands and therefore, the peak is not regarded as reliable bands for the identification of maghemite.

4.1.3 Surface area analysis

Table 4.2 represents the surface area and the sample size for samples G1, G2, G3, G4 and G5. The specific surface area for sample G1, G2, G3, G4 and G5 are 217.77, 115.38, 109.08, 133.49 and 540.54 m^2/g respectively. The smallest sample size is G5 which is 2.41 nm and the largest sample size is G3 which is 12.00 nm. By referring to these results, we can suggest that by increasing the concentration of ferric nitrate to 0.5 M, the sample size is increasing and the sample size will start decreasing if the concentration of ferric nitrate is further increased. The pattern of size for this characterization test is a bit different from other characterization. This might be because powder nanoparticles were used during this test. When drying the nanoparticles, agglomeration between the powders might have occurred. That is why the pattern of the size for this characterization test is different from other test.

The size of the samples was calculated from the equation below:

$$d_{\mathrm{BET}} = \frac{6}{\rho s} \tag{4.3}$$

Where d is the size of the nanoparticles in nm, ρ is the density of the bulk maghemite and s is the specific surface area of the sample obtained from BET analysis.

Table 4.2: Result of BET analysis for all samples

Sample	Specific surface area (m^2/g)	Sample size (nm)
G1	217.77	5.98
G2	115.38	11.30
G3	109.08	12.00
G4	133.49	9.80
G5	540.54	2.41

4.1.4 Particle size and stability

Table 4.3 tabulated the hydrodynamic size by volume of the particles and zetapotential value of sample labelled G1, G2, G3, G4 and G5. The sizes of all samples are around 100 nm. The smallest sample is G3 with hydrodynamic size of 37.78 nm followed by sample G4 with hydrodynamic size of 41.62 followed by G2 with 58.24 nm followed by G1 with 92.95 nm and followed by the biggest sample, G5 with hydrodynamic size of 109.30 nm. This trend is in agreement with XRD and TEM. With this trend, it can be said that samples with the concentration of ferric nitrate more than 0.5 M will yield a bigger size of nanoparticles. Even though the trend is similar, it can be seen that the particle size obtained from zetasizer are larger than the other two experiments. This is due to the hydrodynamic diameter of particles and their surrounding of solvent layers.

Zeta potential is an important tool to predict the long term stability of the nanoparticles. Zeta potential of the particles has values typically range from +100 mV to -100 mV (Nanocpmposix, 2011). According to Malvern (2011), +/- 30 mV can be considered as suitable threshold value for stability. Thus, coagulation will not occur as long as the particle Kinetic Energy does not exceed this barrier. From the data presented in Table 4.3, all sample have zeta potential value of more than +30 mV, thus, we can prove that all samples are stable suspension.

Table 4.3: Hydrodynamic size and zetapotential for all sample

Samples	Hydrodynamic size (nm)	Zeta potential (mV)
G1	92.95	46.80
G2	58.24	45.10
G3	37.78	43.00
G4	41.62	45.90
G5	109.30	49.70

4.1.5 Shape and size analysis

Figure 4.5 (a), (b), (c), (d) and (e) show TEM result for sample G1, G2, G3, G4 and G5, respectively. It can be seen that the particles were spherical in shape, however, aggregation occurred in all the samples. This might be due to poor sample preparation. Figure 4.6 shows the average particle size calculated from TEM analysis. 100 particles were taken in calculating the average size of the maghemite nanoparticles. The largest size is 8.32 nm, which is sample G1 and the smallest size is 6.9 nm which is sample G3. Tartaj *et al.* (2006) also reported that the maghemite nanoparticles are in spherical shape and only few larger particles which are found to be aggregated. The average physical size of TEM image is in a good agreement with XRD crystallite size, which proved that the particles are monocrystals. Nazari *et al.* (2014) also stated in their report that the shape of maghemite nanoparticles obtained from TEM image was spherical with the size less than 20 nm.

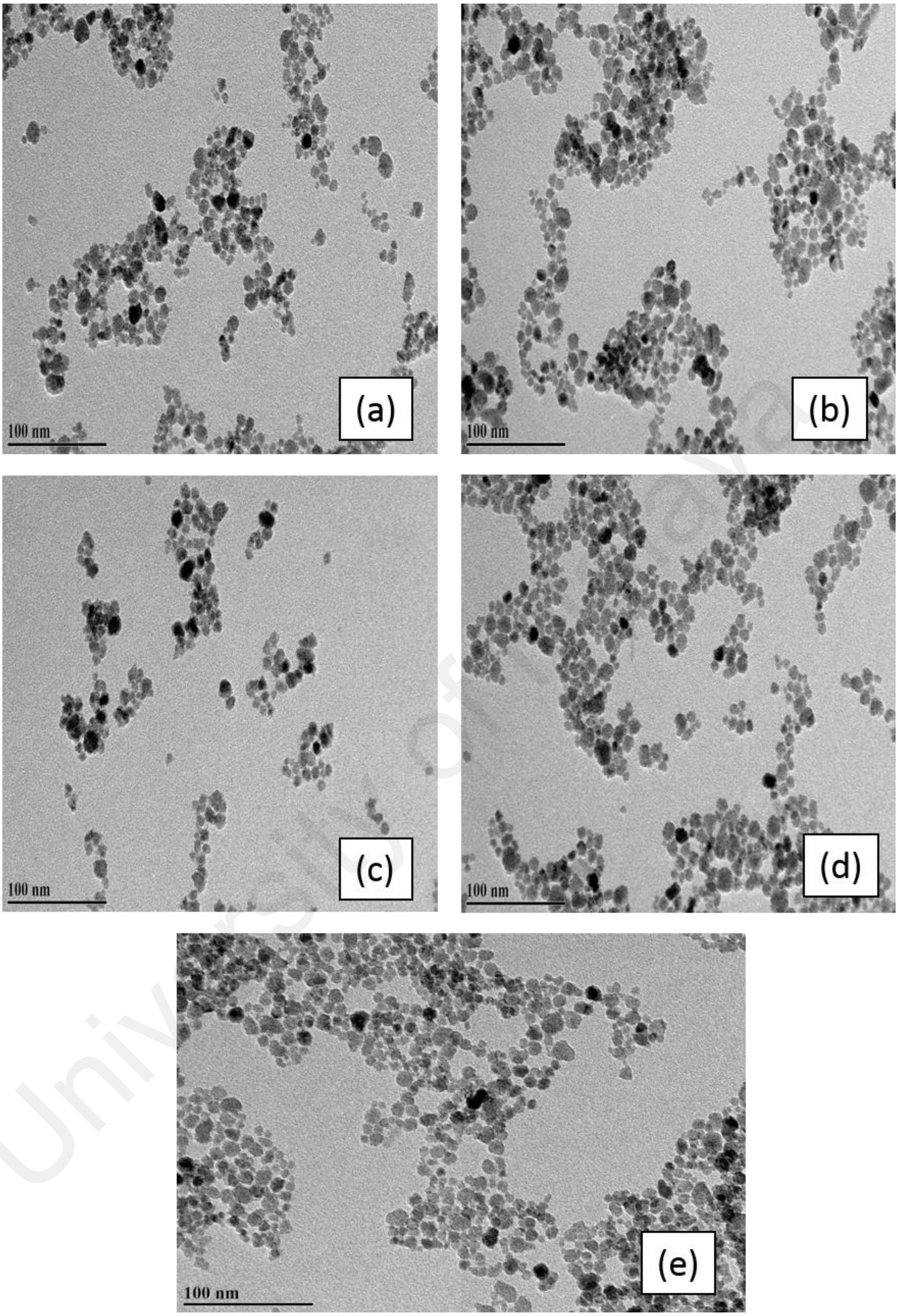

Figure 4.5: TEM images for sample (a) G1, (b) G2, (c) G3, (d) G4 and (e) G5

Figure 4.6 showed a whisker and box plot for all samples. The red line in the middle of the box represents the mean value of the particle size while the black line indicated the median value of 100 particles for each samples. From the box plot, it also showed the minimum and maximum size of the nanoparticles. The dotted line in the box plot represent the outliers (3 x Interquartile or 1.5 x Interquartile). From the box plot, the distributions of the particles for all samples are homogeneous as there is only one peak can be seen. The size range for each samples are varied. The size range for G1 (4 – 16 nm), G2 (3 – 15 nm), G3 (4- 10 nm), G4 (3 – 11 nm) and G5 (5 – 17 nm), the mean obtain shows that G3 has the smallest average particle size which is 6.9 nm with the narrowest size range. This shows that G3 is not only the smallest but the homogeneity in synthesizing a good size in narrow range is achieved too. The other sample average particles size is 8.3, 8.2, 7.3, and 9.6 nm for sample G1, G2, G4 and G5 respectively.

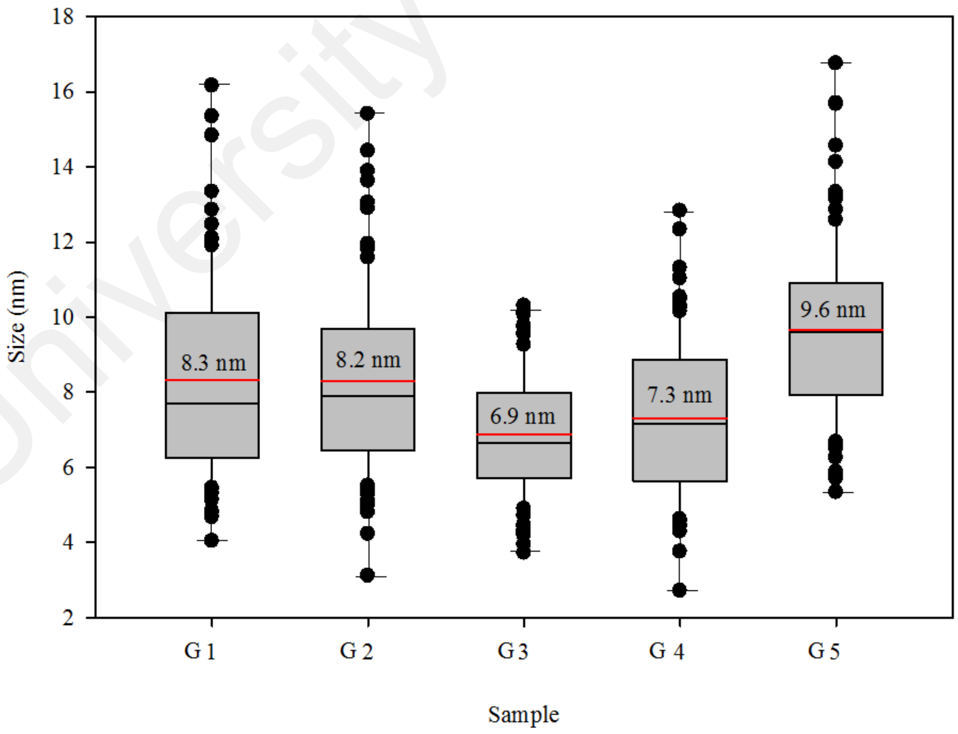

Figure 4.6: Average particle size from TEM analysis

4.1.6 Magnetic analysis

Figure 4.7 shows the magnetization versus applied field curves of all samples at room temperature. It can be observed that all samples exhibit no hysteresis loop and passes through origin, which indicates that the samples are superparamagnetic nanoparticles. The saturation magnetization values obtained at ±10 kOe for sample G1, G2, G3, G4 and G5 are 34.32, 19.52, 29.56, 14.03 and 28.88 emu/g respectively. These values are lower than the saturation magnetization value of bulk maghemite (74 emu/g). This occurrence usually observed in the nanoparticle interacting system. This reduction can be described as the effect arising from broken symmetry and reduced coordination of atom lying on the surface of the maghemite particles (Kluchova *et al.*, 2009). The magnetic size can be calculated from the formula shown:

$$\mathbf{D}_{\mathbf{mag}} = \left[\frac{\mathbf{18}\ \boldsymbol{kT}\ (\frac{\boldsymbol{dM}}{\boldsymbol{dH}})}{\boldsymbol{\pi\rho Ms}^2}\right]^{\mathbf{1/3}} \tag{4.4}$$

Where k is the Boltzmann constant, T is the room temperature, $\frac{dM}{dH}$ is the slope of the magnetization curve nears zero fields, ρ is the maghemite density and M_s is the saturation magnetization. The magnetic size obtained for all samples can be seen in Table 4.4 which the size are 25.4, 23.6, 27.2, 21.0 and 26.9 nm for sample G1, G2, G3, G4 and G5 respectively. Ang *et al.* (2014) stated in their research that superparamagnetic occur when the particle size is below a certain critical dimension which is as small as tens of nanometers. However, in Table 4.4, it can be seen that the magnetic size of all samples are relatively big. This is due to the sample behaviour. To investigate the magnetic properties using AGM, the suspension must be dried in an oven to obtain powder sample. From TEM and zeta potential analysis, it is known that the nanpparticles are stable suspension with relatively small size nanoparticles. However, as the samples is dried, they might actually clumped together and cause some agglomeration and thus, affected their magnetic size dimension.

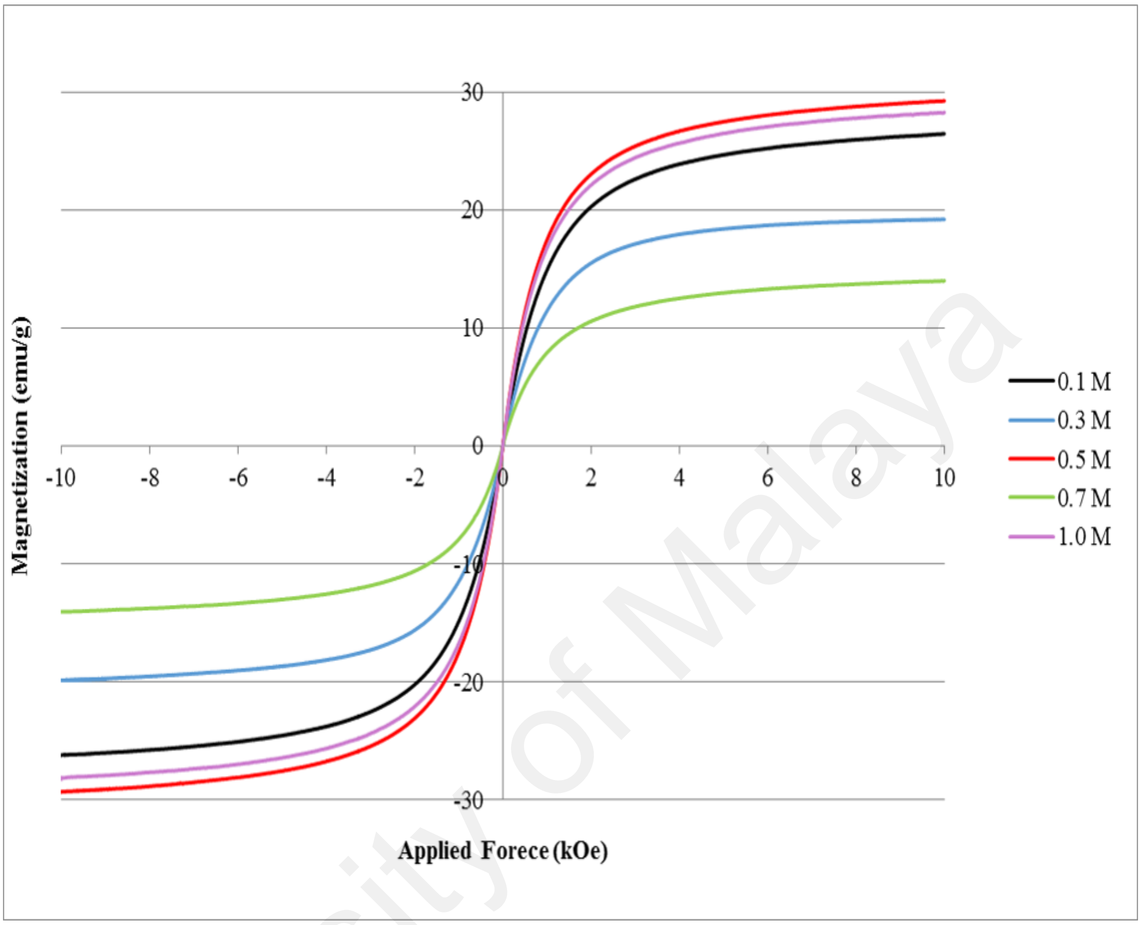

Figure 4.7: Magnetic curves for all samples

Table 4.4: Saturation magnetization, remanence, coercivity and magnetic size for all samples

Sample	Saturation Magnetization, Ms (emu/g)	Remanence, Mr (memu/g)	Coercivity, Hc (Oe)	Magnetic Size (nm)
G1	34.33	98.21	3.19	25.40
G2	19.52	59.91	3.08	23.60
G3	29.57	85.39	2.68	27.20
G4	14.04	40.06	2.80	21.00
G5	28.88	79.17	2.64	26.90

4.1.7 Thermal analysis

Figure 4.8 shows the thermal analysis for all samples at different ferric nitrate concentration. All samples exhibit similar weight loss, where two steps of weight loss can be seen. The weight loss that occured from ambient temperature to approximately 200°C is due to the evaporation of absorbed water and crystalline water from the sample. The remaining weight loss from 200°C to 400°C are due to volatilization of the remaining water bonding in the sample which it will evaporate at water critical temperature of 374°C (Nurdin, 2016).

From the small figure attached to Figure 4.8, it can be seen that the reaction of sample G3 starts earlier compared to other sample. This is attributed to the small size of the particles. Smaller particles tends to reacts faster compared to large particle size.

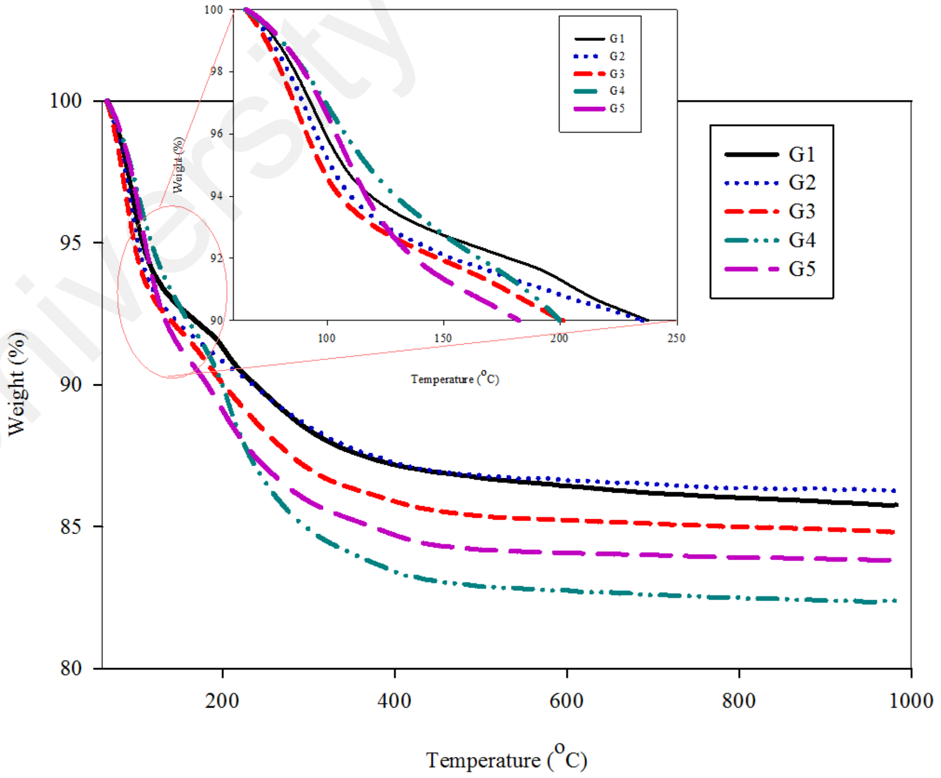

Figure 4.8: TGA curve for all samples

Thus, for stage I, it can be conclude that from microstructural study analysis, it was found that the nanoparticles belongs to maghemite group and it was further confirmed with raman analysis. The size of the maghemite nanoparticles were further confirmed withe specific surface area analysis, zetasizer, and TEM. It was found that the maghemite nanoparticles produced are within 10 nm. The magnetic properties were investigated through AGM and it was revealed that all samples exhibit superparamagnetic behaviour with different magnetic size of the nanoparticles. Thermal analysis exposed that the samples exhibit two steps of weight loss and no existance of other phase except maghemite nanoparticles. From Figure 4.9, by comparing the size from all characterization analysis, sample G3 has the smallest size compared to other sample and thus was chosen to be deposited on the silicon substrate in stage II.

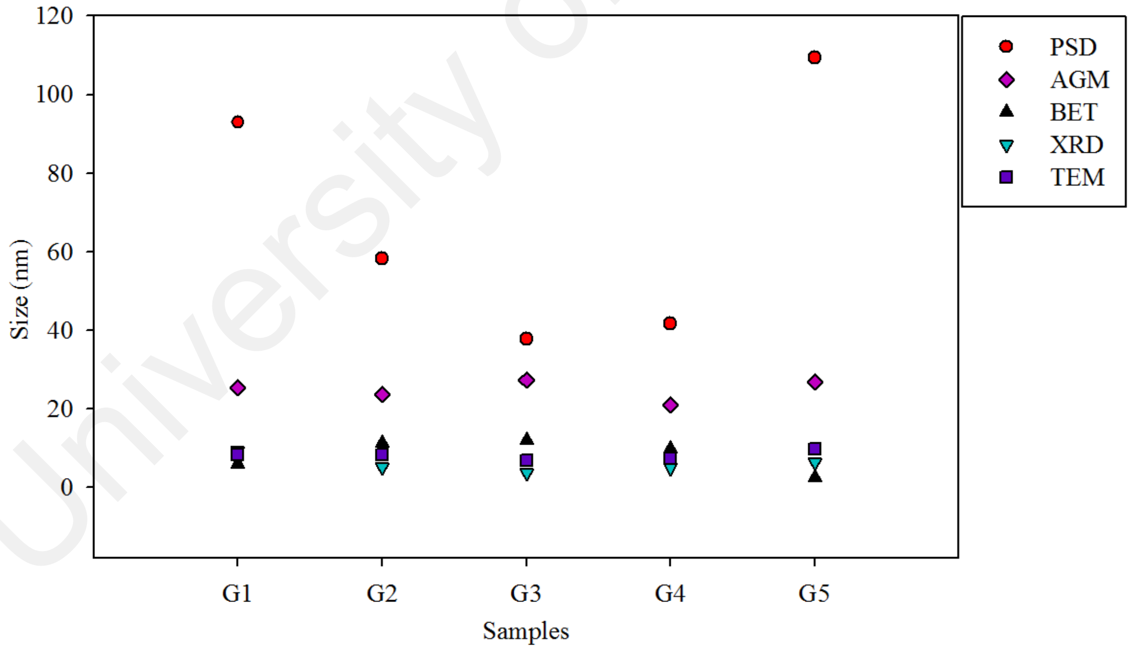

Figure 4.9: Comparison size for all samples in stage I

4.2 Deposition of Maghemite Nanoparticles on Silicon Substrate

4.2.1 J-E Analysis

Figure 4.10 shows the relationship of leakage current density and electrical field for all samples (600°C, 700°C, 800°C and 900°C). This graph was obtained from the current-voltage (I-V) characteristic which then transformed into J-E plot.

It can be seen from Figure 4.10 that sample with annealing temperature of 900°C has the highest electrical breakdown field. While on the other hand, the lowest leakage current density, J, attained by sample with annealing temperature of 600°C. The values for electrical field and leakage current density for all samples were tabulated in Table 4.5.

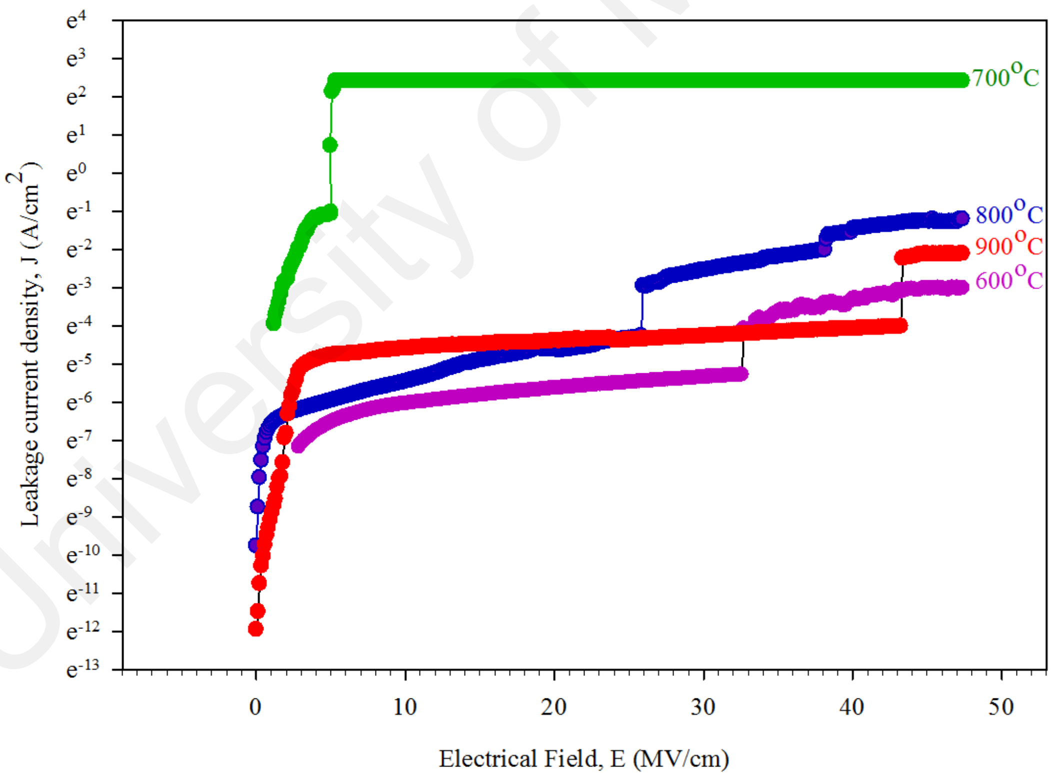

Figure 4.10: J-E characteristic of samples with different annealing temperature (600°C, 700°C, 800°C and 900°C)

Among all the samples, high electrical field value was attained by sample with annealing temperature of 900°C which was 43.3 MV/cm and approximately 25% better than sample annealed at 600°C. On the other hand, low leakage current density attained by sample 600°C which was 3.94×10^{-1} A/cm^2 and it was 1 order of magnitude better than sample annealed at 900°C as shown in Table 4.5.

Table 4.5: Electrical field and leakage current density for all samples

Sample	**E (MV/cm)**	**J (A/cm^2)**
600	32.4	5.49×10^{-3}
700	4.9	3.94×10^{-1}
800	25.6	1.39×10^{-3}
900	43.3	1.83×10^{-3}

This significant observation might be explained due to several reasons which are the grain size of the maghemite nanoparticles, surface roughness exerts by different annealing temperatures, thickness of the nanoparticles thin film, porosity of the annealed samples, distribution and uniformity of the nanoparticles and consolidation behaviour of the nanoparticles at different temperatures. These reasons will be discussed in the next sub chapter.

4.2.2 Microstructural Analysis

Figure 4.11 shows the XRD relationship of relative intensity vs. 2 theta (°) for maghemite nanoparticles thin film on silicon substrate. The samples were prepared by varying the annealed temperature (600°C, 700°C, 800°C and 900°C). The diffraction pattern collected was from 5° to 80°. It can be seen that all samples exhibit almost similar pattern and peaks. The measured peaks are defined at approximately 33°, 62° and 76° for maghemite with miller indices of (220), (440), (533) respectively and 28°, 69° and 76° for silicon with miller indices of (111), (400) and (331) respectively. These peaks were consistent with the standard structure (JCPDS No. 98-008-7119) for maghemite and (JCPDS No. 00-027-1402) for silicon. This shows that maghemite thin films for all samples are stable as they are still in the same phase even though it was annealed up to 900°C.

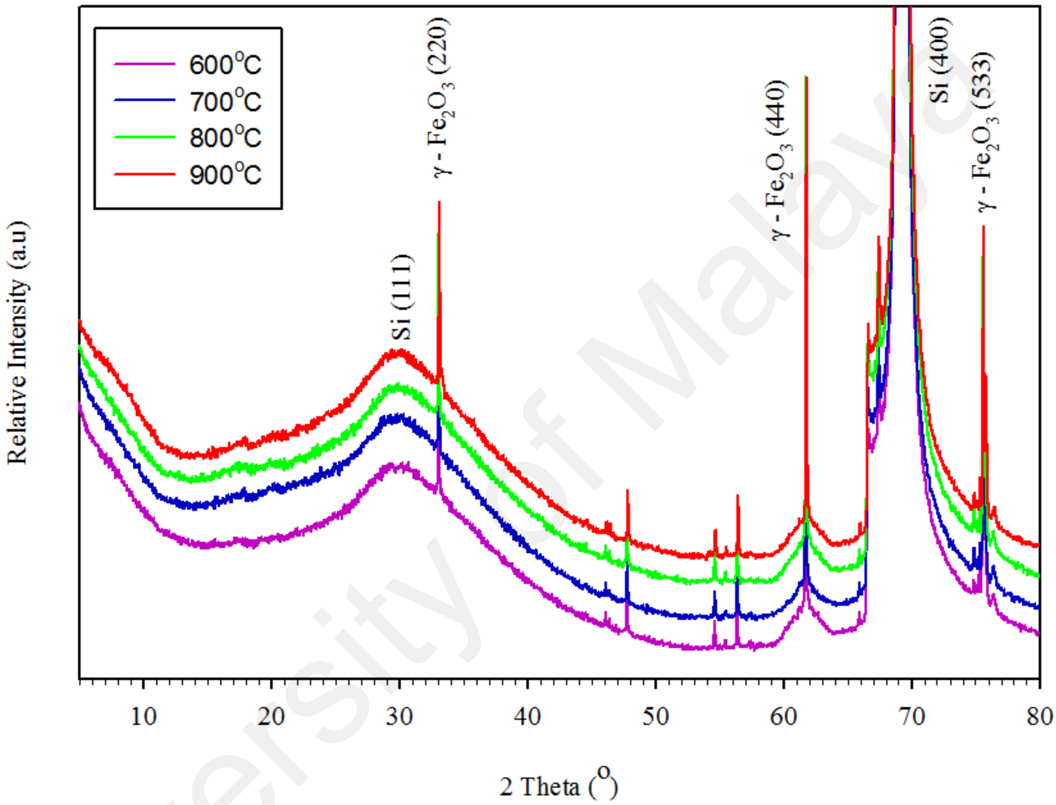

Figure 4.11: XRD pattern for maghemite thin film deposited on silicon substrate

The average crystallite sizes of the samples were calculated from 3 main peaks of maghemite at plane (220), (440) and (533) using Sherrer's equation in equation (4.2).

The average crystallite size calculated before the deposition of maghemite nanoparticles on silicon substrate was 3.59 nm. Nonetheless, after the deposition and annealing process, the crystallite size were found to be three to four times bigger than before the deposition where it can be seen from Figure 4.11, the crystallite size calculated were 10.9 nm, 5.9 nm, 13.6 nm and 13.7 nm for sample 600°C, 700°C, 800°C and 900°C respectively. As the temperature increase from 600°C to 700°C, the size of maghemite nanoparticles on the silicon substrate decrease. However, the size of the nanoparticles start getting bigger as the temperature increased from 800°C to 900°C.

This occurrence was due to the grain growth of the maghemite nanoparticles during the sintering process where the recovery and recrystallization of the nanoparticles were completed.

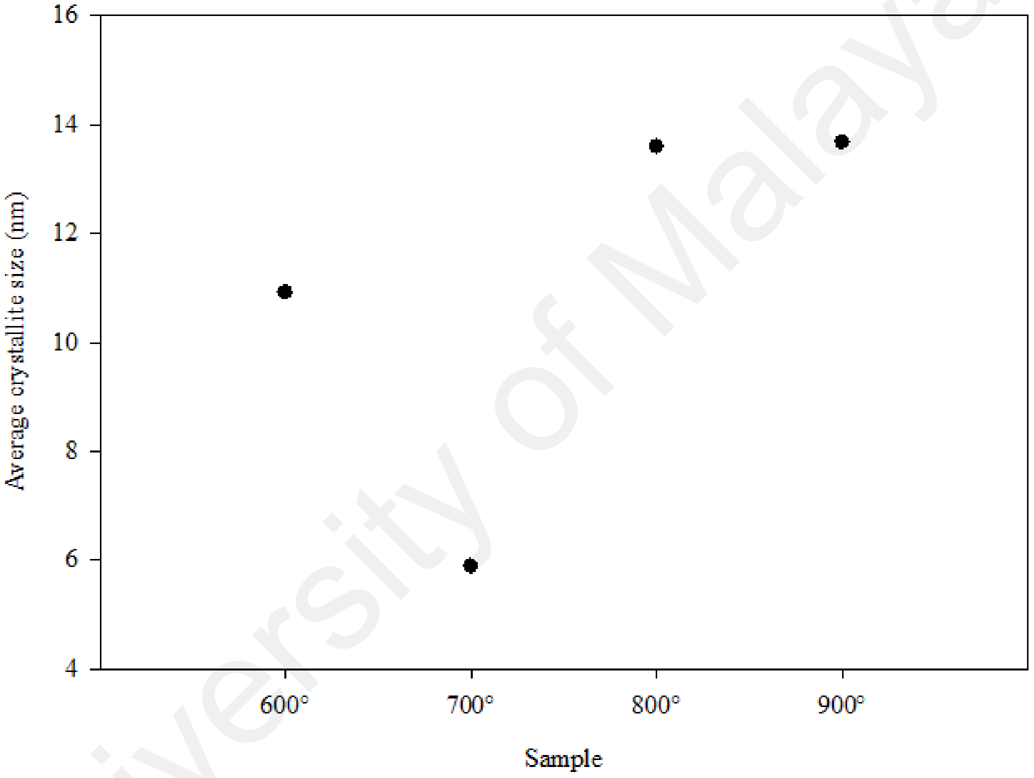

Figure 4.12: Average crystallite size trend for all samples

By comparing the electrical performance of the samples with Figure 4.12, it can be seen that the smallest crystallite size of maghemite nanoparticles worsen the electrical performance while crystallite size between 10.9 – 13.7 nm gives better electrical performance. Sample annealed at 900°C has the largest crystallite size gives optimum electrical breakdown strength with recorded leakage current density of 10^{-2} A/cm^2. On the other hand, sample annealed at 600°C has the crystallite size of 10.9 nm recorded a lower electrical breakdown strength by approximately 25% but improved the leakage current density by an order of magnitude.

This significant circumstance could be explained due to the roughness and porosity of the annealed samples, the distribution, and uniformity and/or consolidation behaviour of the nanoparticles at different annealing temperatures. Through AFM analysis in section 4.2.4, the aforementioned factors can be further explained.

4.2.3 Raman Analysis

Raman spectroscopy is an alternative method to determine the structure of the prepared thin film. This analysis was done to support the result obtained from XRD analysis. Figure 4.13 shows the raman spectra of the maghemite thin film prepared at different annealing temperature (600°C, 700°C, 800°C and 900°C). Schimanke and Martin (2000) reported in their paper that the transformation of maghemite to hematite can be obtained if the nanoparticles are heated above 300°C. However, in Figure 4.13, no traces of main peak of hematite can be found at 225 and 245 cm^{-1} (Hanesch, 2009). The peak at 520 cm^{-1} is assigned to be originated from silicon substrate (Goh *et al.*, 2016). From the graph obtained, it was difficult to observe other peaks as the intensities of the silicon substrate are too high. However, there are slightly peaks around 950 cm^{-1} for all samples. This peak did not belong to maghemite, magnetite, hematite or silicon. Thus, the peak might be inferred to be polycrystalline of interfacial layer (Goh *et al.*, 2016).

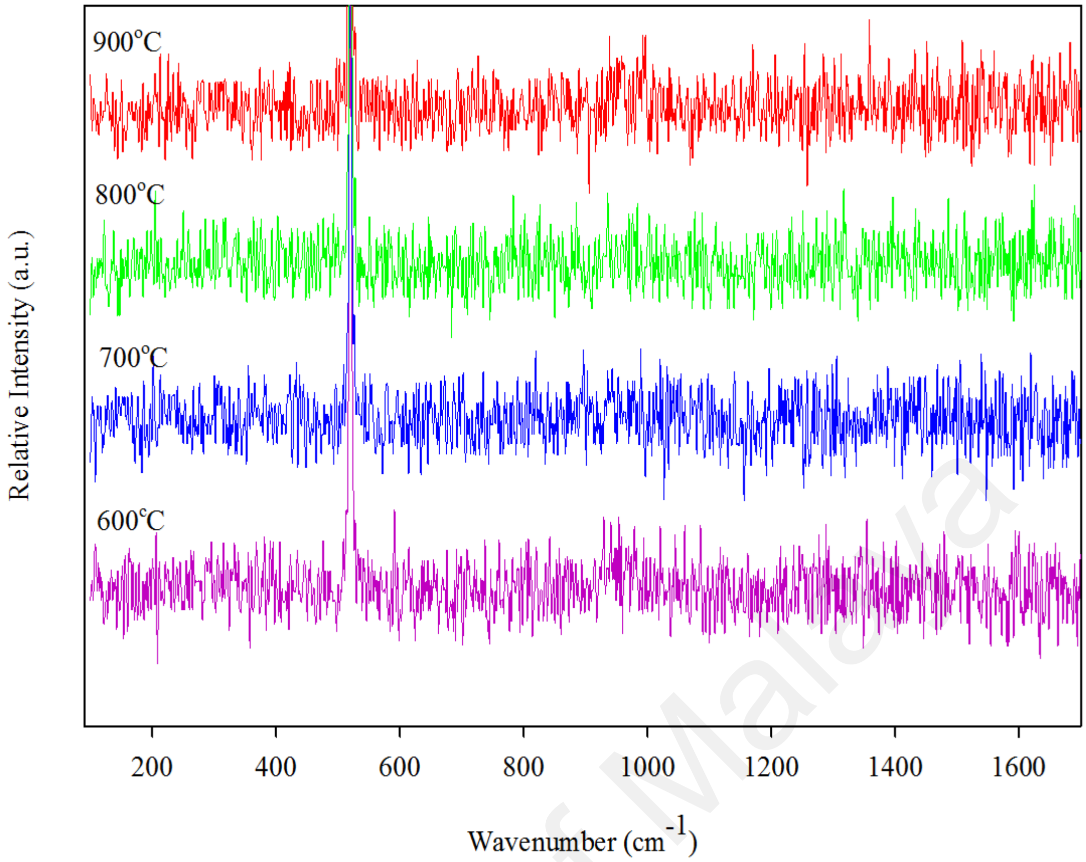

Figure 4.13: Raman spectra for all samples

4.2.4 Surface Morphology Analysis

Figure 4.14 shows two dimensional AFM image in the scanned area of 1µm x 1µm of the thin film of maghemite nanoparticles annealed at different temperature (600°C, 700°C, 800°C and 900°C). It can be seen that the surface of the as-deposited thin film of all samples are smooth and uniform without any foreign features on the surface.

From Figure 4.14, it can be seen that the particles are getting smaller as the temperature increase from 600°C to 800°C. According to Hatalis and Greve (1988), as the annealing temperature increase, the nucleation rate of new grains during the process is also increase. They also stated that the final grain size is determined by the annealing temperature. However, as the temperature increase to 900°C, the nucleation of the grains stopped and the grain growth took place. Low nucleation and high growth rates are affected by high temperature where coarse microstructure with large grains was formed.

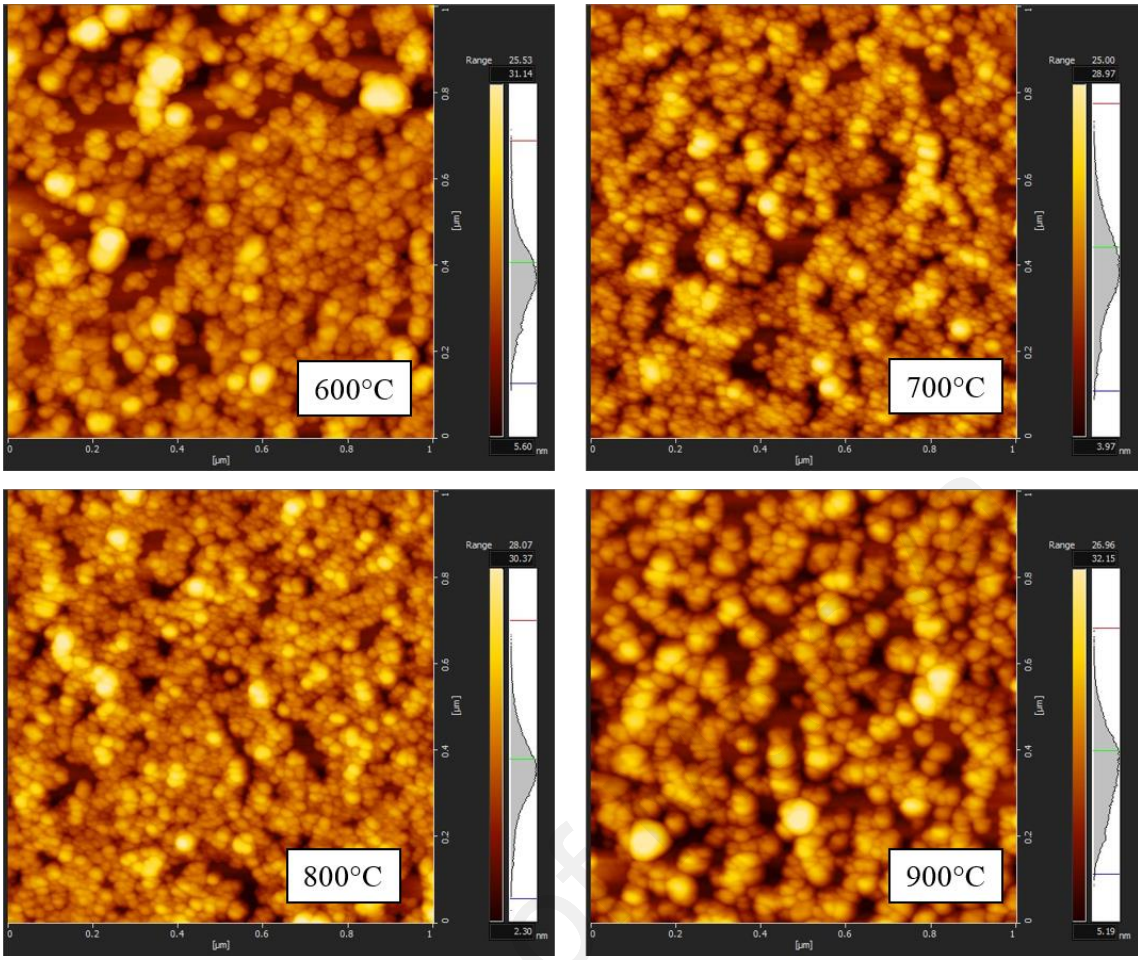

Figure 4.14: AFM images for samples annealed at 600 °C, 700 °C, 800 °C and 900 °C

The surface roughness was observed to be decreasing as the annealed temperature increase from 600 °C to 700 °C due to the nucleation of the nanoparticles**.** However, as the annealing temperature was further increase up to 900 °C, the nucleation has stopped but the grain growth started to take place, thus, the surface roughness increased as shown in Figure 4.15.

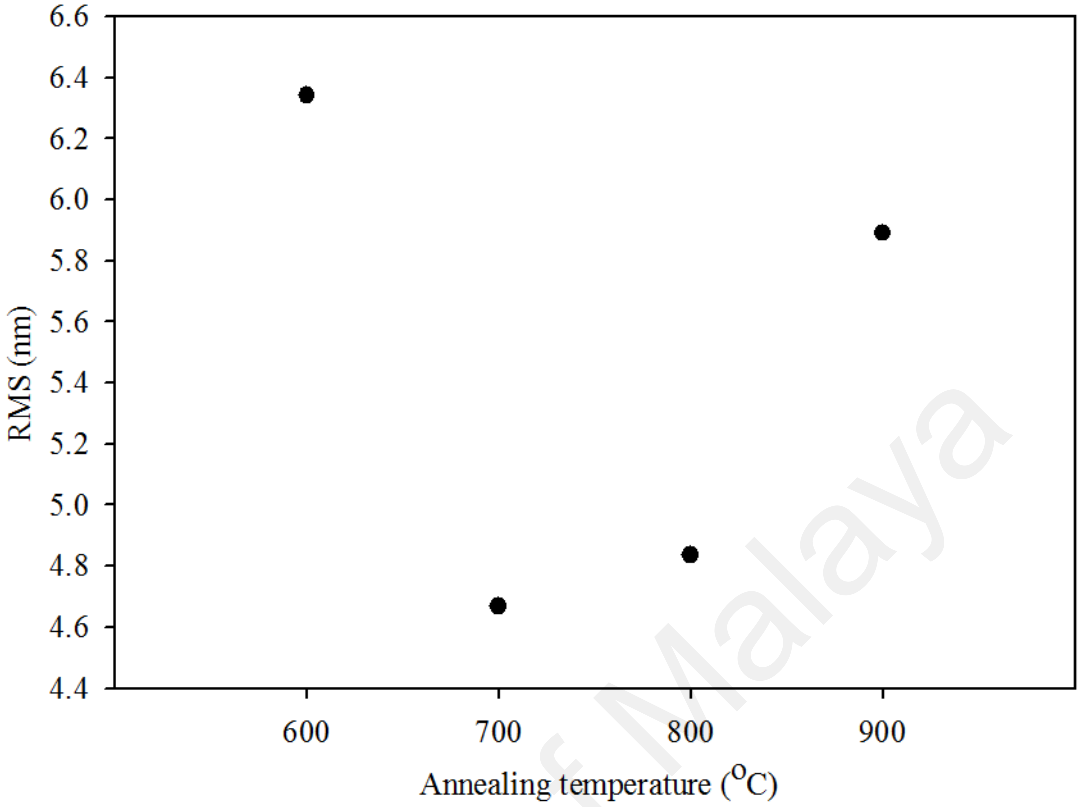

Figure 4.15: Surface roughness trend for samples with different annealing temperature

The thicknesses of the samples annealed at various temperatures are tabulated in Table 4.6. It can be seen that sample with annealing temperature of 900°C has the thickest thin film maghemite nanoparticles which was approximately 38.5 nm, followed by sample annealed at 600°C, 800 and 700°C with the thickness approximately 37.0 nm, 35.5 nm and 30.9 nm respectively. Samples with annealing temperature of 600°C and 900°C have thicker maghemite thin film compare to other samples. Besides, the lowest leakage current density and the highest electrical breakdown value also attained by samples with annealing temperature of 600°C and 900°C, respectively. This proves that thicker maghemite nanoparticles thin film gives better electrical performance.

Table 4.6: Thickness of the nanoparticles thin film measured at different temperatures

Temperature (°C)	Thickness (nm)
600	37.0
700	30.9
800	35.5
900	38.5

Referring to Figure 4.14, it can be seen that the particle distribution, consolidation and porosity plays an important role in electrical characteristic of the samples. Samples with annealing temperature of 700°C and 800°C were seen to have smaller grain size nanoparticles and tight distribution with little porosity. However, the electrical performances is lower than the samples annealed at 600°C and 900°C where it can be seen that the grain size of the nanoparticles were slightly bigger and the particle distribution is quite loose compared to samples annealed at 700°C and 800°C.

Thus, from all the results presented above, it can be seen that the sample with annealing temperature of 900°C have higher electrical breakdown which was 25% better than samples annealed at 600°C while sample with annealing temperature of 600°C has low leakage current density which was 1 order of magnitude better than sample with annealing temperature of 900°C. This was due to their grain sizes and surface roughness which were higher compare to the other two samples with annealing temperature of 700°C and 800°C. Besides that, the thickness of the thin film also plays an important role in electrical performances of the samples. The thicker thin film gives better electrical breakdown where it can be seen from the annealing temperatures of 600°C and 900°C samples.

CHAPTER 5: CONCLUSION

In the first part of the study, investigation on relationship between the size, stability and magnetization of maghemite nanoparticles using different concentration of ferric nitrate was performed. At lower concentration of ferric nitrate (0.1 M, 0.3 M and 0.5 M), the size of maghemite nanoparticles tends to become smaller as the ferric nitrate act as a barrier layer around the nanoparticles and thus preventing the nanoparticles to agglomerate. The smallest size, high stability and high saturation magnetization of maghemite nanoparticles was obtained when the size of the ferric nitrate concentration optimized at 0.5 M which is attained by sample G3. At higher concentration (0.7 M and 1.0 M), ferric nitrate can no longer act as a barrier layer and stimulate the formation of agglomeration. Thus, sample G3 was chosen to be deposited on silicon substrate.

In the second part of the study, the relationship between different annealing temperature (600 °C, 700 °C, 800 °C and 900 °C) and electrical properties of the as-deposited maghemite nanoparticles on silicon substrate was investigated. The sample possess low leakage current and high electrical breakdown is considered the best sample. In this study, sample annealed at 600 °C showed the lowest leakage current density which was 5.49 x 10^{-3} A/cm^2 while sample annealed at 900 °C exhibit the highest electrical breakdown which was 43.3 MV/cm. This occurrence was due to several factors which were the surface roughness and grain size of the as-deposited maghemite nanoparticles.

In conclusion, unmodified maghemite nanoparticle has been successfully synthesized with the size of 6.9 nm with optimum ferric nitrate concentration of 0.5 M, whereas 900 °C is the best temperature that exhibit highest electrical breakdown of the as-deposited maghemite nanoparticle on silicon substrate.

FUTURE WORK

Maghemite nanoparticles are known to have unique properties and also have high dielectric constant value. This study showed that maghemite nanoparticles can be a potential material of oxide layer in the MOS device. However, more studies needs to be conducted to further improve the agglomeration issues and the stability of the nanoparticles in order to improve the electrical performance so that maghemite nanoparticles can be on a par with other existing high-k value materials in the industry.

REFERENCES

Azbarzadeh, A. Samiei, M., and Daravan, S. (2012). Magnetic nanoparticlesL Preparation, physical properties and applications in biomedicine. *Nanoscale Research Letter*, *7*(1):1.

Ang, B. C. and Yaacob, I. I. (2007). Synthesis and characterization of magnetic iron oxide nanoparticles via w/o microemulsion and Masart's procedure. *Journal of materials processing technology, 191*(1): 235-237.

Ang, B. C., Yaacob, I. I. and Chew, C. (2014). Effect of $FeCl_2$ Concentration on the Properties of Magnetic Nanoparticles by Using Massart's Procedure. *Sains Malaysiana, 43*(4): 611-616

Asoka-Kumar, P., Alatalo, M., Ghosh, V., Kruseman, A., Nielsen, B. and Lynn, K. (1996). Increased elemental specificity of positron annihilation spectra. *Physical Review Letters, 77*(10): 2097.

Baliga, B. J. (2010). *Advanced power MOSFET concepts*: Springer Science & Business Media.

Bjelkhagen, H. I. (2013). *Silver-Halide recording materials: For Holography and their processing*. Berlin: Springer Verlag.

Chakraborty, A. (2012). *Magnetism of Nanocrystallizad Amorphous* $Fe_{75}B_{10}Si_{15}$ *(Dissertation).*

Chatterjee, K., Sarkar, S., Rao, K. J. and Pria S. (2014). Core/shell nanoparticles in biomedical applications. *Advances in Collois and Interface Science, 209*: 8-39.

Chaudhari, N., Warule, S., Muduli, S., Kale B., Jouen, S., Lefez, B., Hannoyer, B. and Ogale, S. (2011). Maghemite (hematite) core (shell) nanorods via thermolysis of a molecular solid of Fe-complex. *Dalton Transactions, 40*(31): 8003-8011.

Chi, T., Gouadec, G., Colombam, P., Wang, G., Mazerolles, L. and Liem, N. (2011). Off-resonance Raman analysis of wirtzite CdS ground to the nanoscale: structural and size-related effects. *Journal of Raman Spectroscopy, 42*(5): 1007-1015.

Chikazumi, S. and Graham, C. (1997). *Physics of Ferromagnetism (International Series of Monographs on Physics)*. New York: Oxford University Press.

Classes of Magnetic Materials. (n. d.). Retrieved from http://www.irm.umn.edu/hg2m/hg2m_b/hg2m_b.html

Classifications of Interactions and Types of Magnetism. (n. d.). Retrieved from http://www.tf.uni-kiel.de/matwis/amat/elmat_en/kap_4/backbone/r4_1_3.html

Compaño, R. and Hullmann, A. (2002). Forecasting the development of nanotechnology with the help of science and technology indicators. *Nanotechnology, 13*(3): 243.

Daou, T., Greneche, J., Pourroy, G., Buathong, S., Derory, A., Ulhaq-Bouillet, C., Donnio, B., Guillon, D. and Begin-Colin, S. (2008). Coupling agent effect on magnetic properties of functionalized magnetic-based nanoparticles. *Chemistry of Materials, 20*(18): 5869-5875.

DoITPoms, (n. d.). Types of magnetism. Retrieved from http://www.doitpoms.ac.uk/tlplib/ferromagnetic/types.php

Ferroudj, N., Nzimoto, J., Davidson, A., Talbot, D., Briot, E., Dupius, V., Bée, A., Medjram, M. S. and Abramson, S. (2013). Maghemite nanoparticles and maghemite/silica nanocomposite microspheres as magnetic Fenton catalysts for the removal of water pollutants. *Applied Catalysis B: Environmental, 136*: 9-18.

Frey, N. A., Peng, S., Cheng, K. and Sun, S. (2009). Magnetic nanoparticles: Synthesis, functionalization and applications in bioimaging and magnetic energy storage. *Chemical Society Reviews, 38*(9): 2532-2542.

Galup-Montoro, C. and Schneider, M. C. (2007). *MOSFET modeling for circuit analysis and design.* Singapore: World Scientific.

Goh, K. H., Haseeb, A. and Wong Y. H. (2016). Effect of Oxidation Temperature on Physical and Ekectrical Properties of Sm_2O_3 Thin Film Gate Oxide on Si Substrate. *Journal of ELectronic Materials, 45*(10): 5302-5312.

Grau-Crespo, R., Al Bitai, A. Y., Saadoune, I. and De Leeuw, N. H. (2010). Vacancy ordering and electronic structure of γ-Fe_2O_3 (maghemite): A theroretical inestigation. *Journal of Physics: Condensed Matter, 22*(25): 255401.

Gupta, A. K. and Gupta, M. (2005). Synthesis and surface engineering of iron oxide nanoparticles for biomedical applications. *Biometerials, 26*(18): 3995-4021.

Haensch, W., Nowak, E. J., Dennard, R. H., Solomon P. M., Bryant, A., Dokumaci, O. H., Kumar, A., Wang, X., Johnson, J. B. and Fischetti, M. V. (2006). Silicon CMOS device beyond scaling. *Ibm Journal of Research and Development, 50*(4.5): 339-361.

Hampden-Smith, M. J. and Kodas, T. T. (1995). Chemical vapor deposition of metals: Part 1. An overview of CVD processes. *Chemical Vapor Deposition, 1*(1): 8-23.

Hanesch, M. (2009). Raman spectroscopy of iron oxides and (oxy) hydroxides at low laser power and possible applications in environmental magnetic studies. *Geophysical Journal Internation, 177*(3): 941-948.

Ieong, M., Doris, B., Kedzierski, J., Rim, K. and Yang, M. (2004). Silicon device scaling to the sub-10-nm regime. *Science 306*(5704): 2057-2060.

Islam, M. S., Kusumoto, Y., Kurawaki, J., Abdulla-Al-Mamun, M. and Manaka, H. (2012). A comparative study on heat dissipation, morphological and magnetic properties of hyperthermia suitable nanoparticles prepared by co-precipitation and hydrothermal methods. *Bulletin of Materilas science, 35*(7): 1047-1053.

Josephson, L., Tung, C. H., Moore, A. and Weissleder, R. (1990). High-efficiency intracellular magnetic labeling with novel superparamagnetic-Tat peptide conjugates. *Bioconjugate chemistry, 10*(2): 186-191.

Jung, J. S., Kwon, J. Y., Xianyu, W., Noguchi, T., Jeong, S. H., Jeong, S. W. and Roh, Y. (2006). Study of HfO_2 High-k Gate Oxide for Low-Temperature Poly-Si TFT. *Journal of the Korean Physical Society, 48*: 32-34.

Kahng, D. (1976). A historical perspective on the development of MOS transistors and related device. *IEEE Transaction on Electron Device, 23*(7): 655-657.

Khomutov, G. B. and Koksharov, Y. A. (2009). Organized Ensembles of Magnetic Nanoparticles: Preparation, structure and properties. In Gubin, S. P. (Ed.), *Magnetic Nanoparticles*. Weinheim: Wiley-VCH Verlag.

Kluchova, K., Zboril, R., Tucek, J., Pecova, M., Zajoncova, L., Safarik, I., Mashlan, M., Markova, I., Jancik, D., Sebela, M., Bartonkova, H., Bellesi, V., Novak, P. and Petridis, D. (2009). Superparamagnetic maghemite nanoparticles from solid-state synthesis-their functionalization towards peroral MRI contrast agent and magnetic carrier for trypsin immobilization. *Biomaterials, 30*(15): 2855-2863.

Kusumoto, O., Yokogawa, T., Yamashita, K., Takahashi, K., Kitabatake, M., Uchida, M. and Miyanaga, R. (2002). SiC vertical DACFET (Vertical delta-doped accumulation channel MOSFET). *Materials Science Forum, 383-3*: 1211-1214.

Lee, C. Y., Ho, K. L., Lee, D. J., Su, A. and Chang J. S. (2012). Electricity harvest from nitrate/sulfide-containing wastewaters using microbial fuel cell with autotrophic denitrifier, Psedomonas sp. C27. *International Journal of Hydrogen Energy, 37*(20): 15827-15832.

Lee, S. J., Jeong, J. R., Shin, S. C., Kim, J. C. and Kim J. D. (2004). Synthesis and characterization of iron oxide magnetic nano-particle and their surface modifications. *Journal of magnetism and magnetic materials, 324*(8): 1543-1550.

Loekitowati Hariani, P., Faizal, M., Ridwan, R., Marsi, M. and Setiabudaya, D. (2013). Synthesis and properties of Fe_3O_4 nanoparticles by co-precipitation method to removal procion dye. *International Journal of Environmental Science and Development, 4*(3): 336-340.

Lou, J. D., Zhu L. H., Ma, Y. C. and Li, L. (2006). Ferric (III) nitrate supported on kieselghur: A new reagent for selective oxidation of alcohols. *Synthetic communications, 36*(20): 3061-3064.

Magnetism. (n. d.). Retrieved from http://www.splung.com/content/sid/3/page/magnetism

Magnetite. (n. d.). Retrieved from https://www.esci.umn.edu/courses/1001/minerals/magnetite.shtml

Maruyama, T. and Arai, S. (1992). Aluminium oxide thin films prepared by chemical vapor deposition from aluminium acetylacetonate. *Applied Physics Letter, 60*(3): 322-323.

Massart, R. (1981). Preparation of aqueous magnetic liquids in alkaline and acidic media. *IEEE Transactions on Magnetic, 17*(2): 1247-1248.

Matsui, I. (2005). Nanoparticles for electronic device applications: a brief review. *Journal of Chemical Engineering of Japan, 38*(8): 535-546.

Mattis, D. C. (1981). *The Theory of Magnetism, Vol I.* Berlin: Springer Ser. Solid State Sci.

Mattox, D. M. (1973). Fundamentals of ion plating. *Journal of Vacuum Science & Technology, 10*(1): 47-52.

Mattox, D. M. (2010). *Handbook of physical vapor deposition (PVD) processing.* Elsevier.

Miller, E. L., Paluselli, D., Marsen, B. and Rocheleau, R. E. (2004). Low-temperature reactively sputtered iron oxide for thin film devices. *Thin Solid Films, 466*(1): 307-313.

Mody, V. V., Siwale, R., Singh, A. and Mody H. R. (2010). Introduction to metallic nanoparticles. *Journal of Pharmacy and Bioallied Science, 2*(4): 282.

Mohapatra, M. and Anand, S. (2010). Synthesis and applications of nano-structured iron oxide/hydroxide – a review. *International Journal of Engineering, Science and Technology, 2*(8): 127-146.

Mornet, S., Vasseur, S., Grasset, F. and Duguet, E. (2004). Magnetic nanoparticle design for medical diagnosis and therapy. *Journal of Materials Chemistry, 14*(14): 2161-2175.

Moshfegh, A. (2004). PVD growth method: Physics and Technology. In Physics and Technology of Thin Films: IWTF 2003 (pp. 28-53): World Scientific.

Nazari, M., Ghasemi, N., Maddah, H. and Motlagh, M. M. (2014). Synthesis and characterization of maghemite nanopowders by chemical precipitation method. *Journal of Nanostructure in Chemistry, 4*(2): 1-5.

Osburn, C. and Huff, H. (2002). MOSFET device scaling: a (biased) history of gate stacks. *FUTURE, 2000*: 2020.

Oswal, R. R. (2014). Investigation of Different Dielectric Materials as Gate Insulator for MOSFET, 4511: Electronic Theses and Dissertation (Masters Dissertation). Retrieve from Stars – University of Central Florida.

Pankhurst, Q. A., Connolly, J., Jones, S. K. and Dobson, J. (2003). Applications pf magnetic nanoparticles in biomedicine. *Journal of Physics D: Applied Physics, 36*(13): R167.

Park, J. H. and Sudarshan, T. (Eds.) (2001). *Chemical vapor deposition.* ASM International.

Park, W. I., Kim, J. S., Yi, G. C., Bae, M. and Lee, H. J. (2004). Fabrication and electrical characteristic of high-performance ZnO nanorod field-effect transistor. *Applied Physics Letters, 85*(21): 5052-5054.

Pierson, H. O. (1990). *Handbook of chemical vapor deposition: principle, technology and applications.* USA: Noyes Publications.

Ritter, K, Odziemkowski, M., Simpgraga, R., Gillham, R. and Irish, D. (2003). An in situ study of the effect of nitrate on the reduction of trichloroethylene by granular iron. *Journal of Contaminant Hydrology, 65*(1): 121-136.

Robertson, J. (2004). High dielectric constant oxides. *The European physical journal applied physics, 28*(3): 265-291.

Sahoo, S., Agarwal, K., Singh, A., Polke, B. and Raha, K. (2010). Characterization of α-Fe_2O_3 nano powders synthesized by emulsion precipitation-calcination route and rheological behaviour of α-Fe_2O_3. *International Journal of Engineering, Sience and Technology, 2*(8): 118-126.

Salamanca-Buentello, F., Persad, D. L., Martin, D. K., Daar, A. S. and Singer, P. A. (2005). Nanotechnology and the developing world. *PLos Med, 2*(5): e97.

Schimanke, G. and Martin, M. (2000). In situ XRD study of the phase transition of nanocrystaline maghemite (γ-Fe_2O_3) to hematite (α-Fe_2O_3). *Solid State Ionics, 136-137*: 1235-1240

Schwertmann, U. and Cornell, R. M. (2008). *Iron Oxides in the laboratory.* Weinheim: John Wiley & Sons.

Skumryev, V., Stoyanov, S., Zhang, Y., Hadjipayanis, G., Givord, D. and Nogues, J. (2003). Beating the superparamagnetic limit with exchange bias. *Nature, 423*(6942): 850-853.

Smith, W. F. and Hashemi, J. (2006). *Foundations of materials science and engineering.* New York: McGraw-Hill.

Sotiriou, G. A., Blattman, C. O. and Pratsinis, S. E. (2013). Flexible, multifunctional, magnetically actuated nanocomposite films. *Advanced Functional Materials, 23*(1): 34-41.

Sreeja, V. and Joy, P. (2007). Microwave-hydrothermal synthesis of γ-Fe_2O_3 nanoparticles and their magnetic properties. *Materials research bulletin, 42*(8): 1570-1576.

Stevens, P. D., Li, G., Fan, J., Yen, M. and Gao, Y. (2005). Recycling of homogeneous Pd catalysts using superparamagnetic nanoparticles novel soluble supports for Suzuki, Heck and Sonogashira cross-coupling reactions. *Chemical Communications,* (35): 4435-4437.

Tartaj, P., Morales, M. P., Veintemillas-Verdaguer, S., Gonzales-Carreño, T. and Serna, C. J. (2006). Synthesis, properties and biomedical applications of magnetic nanoparticles. In Buschow K. J. H. (Ed.), *Handbook of Magnetic Materials* (pp. 403-482). Netherlands: Elsevier B. V.

The Mineral Hematite. (n. d.). Retrieved from https://www.minerals.net/mineral/hematite.aspx

TU Clausthal. (2016). High-K oxides for new generations of transistors. Retrieved from https://www2.pt.tu-clausthal.de/atp/projects/high-k.html

Tural, B., Özenbaş, M., Atalay, S. and Volkan, M. (2008). Rapid synthesis and characterization of maghemite nanoparticles. *Journal of Nanoscience and Nanotechnology, 8*(2): 861-866.

Vidal-vidal, J., Rivas, J. and Lopez-Quintela, M. (2006). Synthesis and monodisperse maghemite nanoparticles by the microemulsion method. *Colloids and Surfaces A: Physicochemical and Engineering Aspects, 288*(1): 44-51.

Wahajuddin, S. A. (2012). Superparamagnetic iron oxide nanoparticles: magnetic nanoplatforms as drug carriers. *International Journal of nanomedicine, 7*: 3445.

Wilk, G., Wallace, R. and Anthony, J. (2000). Hafnium and zirconium silicates for advanced gate dielectrics. *Journal of Applied Physics, 87*(1): 484-492.

Wu, W., Xiao, X., Zhang, S., Zhou, J., Fan, L., Ren, F. and Jiang, C. (2010). Large-scale and controlled synthesis of iron oxide magnetic short nanotubes: shape, evolution, growth mechanism and magnetic properties. *The Journal of Physical Chemistry C, 114*(39): 16092-16103.

Wu, Z. G. and Gao, J. F. (2012). Synthesis of γ-Fe_2O_3 nanoparticles by homogeneous co-precipitation method. *Micro & Nano Letters, 7*(6): 533-535.

Xie, K., Li, J., Lai, Y., Lu, W., Zhang, Z. A., Liu, Y., Zhou, L. and Huang, H. (2011). Highly ordered iron oxide nanotube arrays as electrodes for electrochemical energy storage. *Electrochemistry Communications, 13*(6): 657-660.

Xu, P., Zeng, G. M., Huang, D. L., Feng, C. L., Hu, S., Zhao, M. H., Lai, C., Wei, Z., Huang, C., Xie, G. X. and Liu, Z. F. (2012). Use of iron oxide nanomaterials in wastewater treatment: A review. *Science of the Total Environment, 424*: 1-10.

Zeng, Q., Oganov, A. R., Lyakhov, A. O., Xie, C., Zhang, X., Zhang, J., Zhu, Q., Wei, B., Grigorenko, I., Zhang, L. and Cheng L. (2014). Evolutionary search for high-k dielectric materials: Methodology and applications to hafnia-based oxides. *Acta Crystallographica Section C: Structural Chemistry, 70*(2): 76-84.

Zhong, L. S., Hu, J. S., Liang, H. P., Cao, A. M., Song, W. G. and Wan, L. J. (2006). Self-assembled 3D flowerlike iron oxide nanostructures and their application in water treatment. *Advanced Materials, 18*(18): 2426-2431.

Zhou, Z., Wu, C., Liu, H., Zhu, X., Zhao, Z., Wang, L., Xu, Y., Ai, H. and Gao, J. (2015). Surface and interfacial engineering of iron oxide nanoplates for highly efficient magnetic resonance angiography. *ACS Nano, 9*(3): 3012-3022.

LIST OF PUBLICATIONS AND PAPERS PRESENTED

Athirah, A. H. N., Chin, A. B., Hoong, W. Y., Hoong, O. B., & Aqilah, B. A. (2018). Synthesis and characterization of γ-Fe2O3 NPs on silicon substrate for power device application. *Materials Research Express, 5*(6), 065020.